AFRL-SN-HS-TR- 2002-042

REAL TIME HOLOGRAPHIC IMAGE PROCESSING

Tufts University
Mark Cronin-Golomb
4 Colby Street
Medford MA 02155

FINAL REPORT: July 1995-June 1996

APPROVED FOR PUBLIC RELEASE: DISTRIBUTION UNLIMITED

AIR FORCE RESEARCH LABORATORY
Sensors Directorate
80 Scott Dr
Hanscom AFB MA 01731-2909

20021129 081

TECHNICAL REPORT

Title: Real Time Holographic Image Processing

PUBLICATION REVIEW

This report has been reviewed and is approved for publication:

APPROVED:

CHARLES WOODS
AFRL/SNHC
Optoelectronic Technology Branch
Electromagnetics Technology Division

APPROVED:

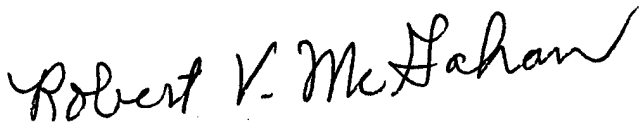

ROBERT V. McGAHAN
Technical Advisor
Electromagnetics Technology Division

REPORT DOCUMENTATION PAGE

Form Approved
OMB No. 0704-0188

Public reporting burden for this collection of information is estimated to average 1 hour per response, including the time for reviewing instructions, searching existing data sources, gathering and maintaining the data needed, and completing and reviewing the collection of information. Send comments regarding this burden estimate or any other aspect of this collection of information, including suggestions for reducing this burden, to Washington Headquarters Services, Directorate for Information Operations and Reports, 1215 Jefferson Davis Highway, Suite 1204, Arlington, VA 22202-4302, and to the Office of Management and Budget, Paperwork Reduction Project (0704-0188), Washington, DC 20503.

1. AGENCY USE ONLY *(Leave blank)*	2. REPORT DATE	3. REPORT TYPE AND DATES COVERED
	1 November 1996	FINAL 1 July 1995 - 30 June 1996

4. TITLE AND SUBTITLE
Real Time Holographic Image Processing

5. FUNDING NUMBERS
C-F30602-95-1-0026
PE - 61102F
PR - E-5-7221
PROJ - 2305
TA - D7
WU - P5

6. AUTHOR(S)
Jehad Khoury, Mark Cronin-Golomb

7. PERFORMING ORGANIZATION NAME(S) AND ADDRESS(ES)
Tufts University
4 Colby Street
Medford, MA 02155

8. PERFORMING ORGANIZATION REPORT NUMBER

9. SPONSORING/MONITORING AGENCY NAME(S) AND ADDRESS(ES)
Charles Woods
AFRL/SNHC
80 Scott Drive
Hanscom AFB, MA 01731-2909

10. SPONSORING/MONITORING AGENCY REPORT NUMBER
AFRL-SN-HS-2002-042

11. SUPPLEMENTARY NOTES

12a. DISTRIBUTION AVAILABILITY STATEMENT
Approved for public release; distribution unlimited.

ESC-02-0975 8 Nov 2002

12b. DISTRIBUTION CODE
a

13. ABSTRACT *(Maximum 200 words)*

We have proposed homodyne and heterodyne techniques for imaging in a scattering medium. The first technique is based on the principle of the Doppler shift difference of the light which is scattered from an object vs light scattered by the surroundings. We showed that the principle of Doppler shift difference, and the principle of first arriving light are similar. However, in contrast to first light, which requires ultrafast pulses, here modulated CW can be used. We also experimentally demonstrated the basic principle for a simple case of an object outside of the scattering medium. The second is an extension of the principle of photon density waves, using a two-dimensional (non-scanning) detection scheme.

14. SUBJECT TERMS	15. NUMBER OF PAGES
holographic	75
	16. PRICE CODE

17. SECURITY CLASSIFICATION OF REPORT	18. SECURITY CLASSIFICATION OF THIS PAGE	19. SECURITY CLASSIFICATION OF ABSTRACT	20. LIMITATION OF ABSTRACT
UNCLASSIFIED	UNCLASSIFIED	UNCLASSIFIED	SAR

Standard Form 298 (Rev. 2-89) (EG)
Prescribed by ANSI Std. 239.18
Designed using Perform Pro, WHS/DIOR, Oct 94

Table of Contents.

1.1 BACKGROUND

We proposed to initiate a program of research in real-time holographic image processing. In this effort new device architectures were proposed, supported by an experimental demonstration and theoretical investigation.

The new applications which we worked on were speckle velocimeters, incoherent-to-coherent nonlinear joint transform correlators, and imaging within a scattering medium using homodyne detection in real-time holography.

For developing these projects in nonlinear holographic image processing, it is necessary to study:(a) the coupled wave theory in real-time holographic devices(1) ;(b) the scattering effects from specific cases of random moving media(2); and (c) the effects of holographic nonlinearites on spatial and temporal signals using the nonlinear transform method (3). Our nonlinear holographic image processor used mainly two devices:(a) An incoherent-to-coherent convertor (4); (b) A real time holographic homodyne and heterodyne detector(5,6).

1.2 PROGRAM OBJECTIVES AND GOALS

The program's objective and goals were to use real-time holographic media, such as photorefractives(1) and bacteriorhodopsin(2), to understand their nonlinearities and then to use these nonlinearities to implement various image processing algorithms. In our implementation we used two main devices: (a) The incoherent-to-coherent detector; (b) The real-time holographic homodyne and heterodyne detector.

INCOHERENT-TO-COHERENT CONVERTOR

The incoherent-to-coherent converter(18) acts like a negative exposure film. For low intensities it behaves as a square law receiver and for large intensities it behaves as a saturated square law receiver. This characteristic may be used to implement the nonlinear joint transform correlator(7,8,9).

HOLOGRAPHIC HOMODYNE AND HETERODYNE DETECTOR

Mixing any two rapidly-varying fields in any real-time holographic medium is always accompanied with time integrative behavior. This time integration behavior is the origin of homodyne and heterodyne detection (10,11,12). In electronics homodyne and heterodyne detection is the basis for designing many devices such as the time integrative correlator, frequency division demultiplexing, lock-in amplifier and notch filter. All these electronic applications can be implemented serially as well as

spatially using real-time holography. We will use the holographic lock-in amplifier(10,12) for detecting images imbedded in noise and we will use the homodyne detector in four-wave mixing for speckle velocimetry.

1.3 TECHNICAL PROGRAM SUMMARY

1.3 (a) Inverse Nonlinear Joint Transform Correlator.

Pattern identification using optical correlators can play an important role in applications, such as target recognition and robotics vision. Two main approaches have been used to design the optical correlator. The first one is based on the Vander Lugt correlator geometry, the second is based on the joint transform correlator JTC geometry.

The second approach is more convenient in the sense that there is no need to fabricate holographic filters, such as the phase-only filter or the matched filter. The original joint transform correlator required a square-law receiver in the Fourier plane(13). This was the basis of all the subsequent designs of the opto-electronic JTCs(9). In contrast, real-time holographic implementation of the JTC was more like the vander-Lugt in terms of its transfer function. Only recently we implemented the first holographic joint transform correlator based on a square-law receiver in the Fourier plane (7,8). Square law nonlinearites can be implemented in various forms. Our specific implementation will use the incoherent-to-coherent converter(4). The square-law nonlinearity in the incoherent-to-coherent convertor has a

saturative behavior like a negative exposure film. This fact makes the incoherent-to-coherent convertor an ideal device for implementing the nonlinear joint transform correlator. There are two advantageous features of our correlator: it will have a reduced DC peak and the joint spectrum saturation can be reached easily by using different wavelengths for erasure of the grating.

1.3(b) Speckle velocimeter.

A speckle velocimeter is a device of interest for metrological applications. In the past, various schemes have been used for these purposes. Some of these schemes used the algorithm of zero-crossing rates(14) , others used measurement of the autocorrelation function; while others used lock-in electronic holography. Only three publications using real-time holography are available in the literature for these purposes(15,16,17). In all these techniques, the processing was in real time. However, the data needs further computer processing. We propose an alternative technique which is based on using the holographic homodyne and heterodyne detection(10,12) as time correlation motion detection(17). In this technique we expect to have a direct measurement of the velocity or the angular velocity without any further processing.

1.3(c) Imaging in scattering media

Imaging in scattering media is one of the most challenging problems in optical signal processing. Holography is one way that appears quite promising. In fact, there is a variety of holographic

methods that may be used for imaging in scattering media.

The earliest approach for imaging in scattering media was due to Duguary and Mattick (1971) who used the principle of the first arriving light (18). In this technique a pulse of light bearing an image passes through the scattering medium. The light that scatters least emerges first; whereas, light that scattered more emerges later. Through time grting it was possible to filter the scattered light . Both real-time holography and electronic holography have been used for these purposes. Only the unscatterd light can interfere with the plane wave and form a hologram. We suggest an alternative technique for imaging within the scattering medium. This technique is based on using the real time hologram as a spatial lock-in detector.

1.4 REFERENCES:

(1) Mark Cronin-Golomb, Baruch Fisher, Jeffry O. White and Amnon Yariv, "Theory and applications of four wave mixing in photorefractive materials," Vol QE-20 (1984).

(2) Brian Cairns and Emil Wolf, "Changes in the spectrum of light scattered by moving diffuser plate,"J. Opt. Soc Am. A. 13. 1922-1928, (1991).

(3) J. W. Goodman "Introduction to fourier optics, (McGraw-Hill, New York 1967).

(4) "Photorefractive incoherent-to-coherent convertor "Y. Shi, D.Psaltis, A. Marrachiki and A. R. Tanguay, J.r., "Appl. Opt. ,22, 3665-3667 (1983).

(5) J. Khoury, Vincent Ryan, Charles Woods and Mark Cronin-Golomb, "Photorefractive optical lock in detector," Opt. Letts. 16, 1442-1444, (1991).

(6) J. Khoury, Mark Cronin-Golomb and Charles Woods. "Real-time holographic frequency division demultiplexing: theoretical aspects," Appl. Opt. 33, 5390-5395 (1994)

(7) J. Khoury, Jonathan S. Kane, George Asimellis, Mark Cronin-Golomb and Charles Woods, "All optical nonlinear joint transform

correlator," Appl. Opt. 33, 8216-8225 (1994).

(8) J. Khoury, M. Cronin-Golomb, P. D. Gianino and C. L. Woods, "Photorefractive two-beam coupling nonlinear joint transform correlator," JOSA:B, 11, 2167-2174, (1994)

(9) B. Javidi, "Nonlinear joint power base optical correlator," Appl. Opt., 28, 2358-2367 (1989)

(10) J. Khoury, V. Ryan, M. Cronin-Golomb and C. L. Woods," Photorefractive frequency convertor and phase sensitive detector," J. Opt. Soc. Am. B. 10, 72-82,(1993)

(11) G. H de Monchenault and G. P. Huignard, "Two-wave mixing with modulated signals in $Bi_{12}Si_{12}O_{20}$ crystal," Appl. Phys. Lett. 50, 1749-1796 (1987)

(12) J. Khoury, V. Ryan, C. L. Woods and M. Cronin- Golomb, "Photorefractive optical lock-in detector," Opt. Lett, 16. 1442-1444 (1991)

(13) C. S. Weaver and J. W. Goodman, "Technique for optically convolving two functions," Appl. Opt. 5, 1248-1249 (1966)

(14) Richard Barakat, "Zero-crossing rate of differentiated speckle intensity,". JOSA:A ,11, 671-673, 1994.

(15) H. J. Tizian, K. Leohnhard and J. Klent,"Real-time displacement and tilt analysis by a speckle analysis technique using BSO crystal," Opt. Commun. 34,327-331 (1980)

(16) Kiyoshi Nakagawa, and Takumi Minemoto. "Read out properties of the specklegram recorded in photorefractive," BSO Appl. Opt. ,30, 2386-2392 (1991)

(17) Steven H. Collicott and Lambertus Hesselink, "Real time photorefractive recording and optical processing for speckle velocimetry," Opt. Letts. 348-350 (1988)

(18) M. A. Duguary and A. T. Mattic, "Ultrafast-speed photography of picosecond light pulses and echoes,"Appl. Opt. 10, 2162-2170, 1971.

Chapter 2

Incoherent Erasure Joint Transform Correlator

2.1.0 Abstract

We propose a nonlinear joint transform correlator which is produced from the erasure of a real time hologram by the joint transform spectrum. Our analysis of this incoherent erasure correlator with a four wave mixing read-out arrangement indicates that the performance of this correlator exceeds that of the phase only correlator

2.1.1 Introduction

We have recently introduced a new class of real-time holographic nonlinear joint transform correlators (JTC) operating on soft-clipping quadratic transfer functions [1-2]. These correlators tune from the matched-filter to the phase-extraction limit and enhance signal detection in noisy environments by compressing the spectra of both the signal and the noise.

Our first approach was based on energy transfer in a two-beam coupling JTC(TBCJTC) [1] using barium titanate. However, many fast real-time holographic materials, such as polymers and certain geometries of multiple quantum wells, cannot be used in this device because they do not produce two-beam coupling. Our second approach was based on four-wave mixing [2] as an alternative to two-beam coupling, utilizing a self-pumped phase-conjugator to retroreflect the joint spectra. This geometry is not attractive because efficient self-pumped phase conjugation is slow.

We therefore propose the incoherent erasure JTC (IEJTC) based on the incoherent erasure of real-time holograms [3] and incoherent-to-coherent conversion [4]. Our analysis shows that the IEJTC operates with a tunable nonlinearity which can be adjusted to operate from the matched filter to the phase extraction limit (or inverse filter), in a fashion similar to our previous approaches [1-2]. The nonlinear transfer function of the IEJTC is controlled by the joint spectral intensity at the Fourier plane. The

classical matched filter is produced in the joint transform low intensity limit, while the inverse filter is produced in the joint transform high intensity limit. Such tunability is very important for detecting signals in various noise environments. For example, the matched filter has proven to be effective for additive Gaussian noise [5] but fails to detect signals in clutter that can be detected by the phase only filter [6].

The main operating improvements of the IEJTC are the increased speed and reduced noise provided by the use of a second wavelength for the erasure (incoherent) beam. Using a shorter wavelength for the erasure light enables fast, low power nonlinear operation into the saturation region, and allows easy separation of any erasure light noise from the correlation signal.

2.1.2 Background and Device Theory

A proposed experimental set-up is shown in Fig. 1: A temporally coherent set of beams of wavelength λc establishes a four-wave-mixing arrangement. Beams 1 and 4 write a grating and beam 2 is the readout which produces beam 3, the phase-conjugate output beam. The erasure beam uses temporally incoherent light at the input plane and the spectra of the scene $S(\nu_x, \nu_y)$ and the reference $R(\nu_x, \nu_y)$) are focused on the photorefractive crystal. Here ν_x and ν_y are the spatial frequency coordinates. The generation of charge carriers by the absorption of the joint spectrum erases the existing grating and this erasure depends on

the intensity $|R(\nu_x, \nu_y) + S(\nu_x, \nu_y)|2$.

The incoherent erasure beam is temporally incoherent to the other beams and must have a at least partial spatial coherence to produce the joint transform. This beam may be produced by a variety of optical techniques including those of white light processing. We consider a crystal with coupling coefficient γ, thickness L, and a small absorption coefficient. Before the erasure beam is introduced the phase-conjugate beam amplitude A_{30} for the undepleted pump case is given by [7]:

$$A_{30}=\frac{(A_1A_4^*)A_2}{I_c}\gamma L$$

where A_j is the amplitude of the jth beam and I_c is the sum of the intensities of the coherent beams 1, 2, and 4. The incoherent beam does not couple with the existing beams due to strong violation of the Bragg conditions, but the total absorbed intensity increases. Considering a monochromatic source (e.g. a second laser) of wavelength λ_i , the modulated phase-conjugate beam amplitude is given by:

$$A_3(\nu_x, \nu_y)=\frac{(A_1A_4^*)A_2\gamma l}{I_c+I_iZ_{\alpha,\lambda}\frac{|R(\nu_x, \nu_y)+S(\nu_x, \nu_y)|^2}{(\lambda_i f_1)^2}}$$

where I_i is the incoherent intensity (of the erasure beam) before the input plane, f1 is the transform lens focal length, and $Z_{\theta,\lambda}$ is a dimensionless factor which depends on the absorption coefficients and wavelengths of the incoherent and coherent beams and can strongly enhance the incoherent erasure.

The modulation depth $d(\nu_x, \nu_y)$, which describes the phase-conjugate beam amplitude modulation by the spectral energy, is obtained by setting:

$$A_3 + A_{30}[1 - d(\nu_x, \nu_y)]$$

Then one can show that:

$$d(\nu_x, \nu_y) = \frac{m_e E(\nu_x, \nu_y)}{1 + m_e E(\nu_x, \nu_y)}$$

where $E(\nu_x, \nu_y)$ is the normalized energy spectrum and me is the effective beam ratio. This equation is functionally identical to the low-coupling limit of the transfer function of the four-wave mixing JTC: see for example Eq. (4) in reference [2].
If E_0 is the product of the area of the input plane and its DC component, we define $E(\nu_x, \nu_y)$ and m_e as follows:

$$E(\nu_x, \nu_y) = \frac{|R\nu_x, \nu_y) + S(\nu_x, \nu_y)|^2}{E_0}$$

$$m_e = Z_{\alpha,\lambda} \frac{E_0}{(\lambda_i f_1)} \frac{I_i}{I_c}$$

In Fig. 2 we plot the modulation depth $d(\nu_x, \nu y)$ versus the product $m_{eE}(\nu_x, \nu_y))$, which is the relative spectral energy incident on the crystal. Two distinct patterns are clearly identified: the modulation is linear with small energies, while for large energies it is independent of the signal energy. This soft-clipping saturation commences at the point of inflection, where $me'E = 1$. Since the crystal responds to the product m_{eE}, not just the energy E, the value of m_e substantially affects the way the phase-conjugate beam amplitude is modulated.

For a small beam ratio ($< m_e = 10^{-2}$) we can set $m_e E(\nu_x, \nu y << 1$ for all the spectral energy values and the modulation depth can be approximated as:

$$d(\nu_x, \nu_y) \approx m_e E(\nu_x, \nu_y) .$$

Equation 7 agrees with Fig. 2 in that the modulated beam has a linear dependence with small signal energies. This dependence is typical of the matched filter, whose peaks are simply the

correlation between the reference and the scene.

For a large beam ratio (> me = 10^3) we can set $m_e E(\nu_x, \nu_{y)>>1}$, and the modulation depth can be approximated as:

$$d(\nu_x, \nu_y) \cong 1 - \frac{1}{m_e E(\nu_x, \nu_y)}$$

This response is independent of the signal intensity at the limit me→∞, is equivalent to the inverse filter and leads to phase extraction. As the beam ratio increases the nonlinearity at the Fourier plane is transformed from the matched-filter type (the linear section) to the inverse-filter type (the limiting section). For intermediate beam ratios the portions of the joint spectrum with low energy, the high frequencies, are amplified by the linear region, and the ones with high energy (low frequencies) are deamplified by the limiting region.

2.1.3 Computer Simulation

We ran computer simulations of the IEJTC with A_{30} =1 and m_e set to 10^{-2}, 10^1, and 10^3. We correlated two disks (Fig. 3a), and a tank versus a tank in clutter (Fig. 4a). Figs. 3b-c plot the peak intensity arrays produced by the matched and phase-only filters with the disks. Figs. 3d-f display the peaks produced by the IEJTC. In Fig. 4b-f the corresponding peaks with the tanks are plotted.

The shape of the peaks and the intensity strongly depend on the beam ratio, which verifies the theoretical predictions. The

correlator with small m_e values has characteristics of the matched filter. We note the similar shape of the correlation peaks between the IEJTC with me= 10^{-2} and the matched filter. Both fail to produce a correlation peak with the tank in clutter.

The transformation of the nonlinearity from the matched-filter type to the inverse-filter type is indicated by peak sharpness and intensity that progressively exceed those of the phase-only filter as the beam ratio increases. For example, the correlation peak for the disks produced by the IEJTC with me = 10^3 had PNR [9] 89.66 and intensity 308. The peak produced by the matched filter had PNR 4.75 and intensity 11.3, and the peak produced by the phase-only filter had PNR 22.32 and intensity 13.5.

2.1.4 Conclusion

We have presented a new approach to implement the nonlinear joint transform correlator. The IEJTC is based on the erasure of a four-wave mixing grating in a real-time holographic media. The resulting soft-clipping quadratic transfer function is similar to our previous photorefractive implementations. The operation of these nonlinear correlators can be tuned from classical matched to the phase extraction by appropriate selection of the operating point. In addition, low-power operation may be achieved by the proper choice of the wavelength of the erasure beam.

2.1.5 Figure Captions:

(1) Proposed experimental arrangement.

(2) Modulation depth of the phase-conjugate beam amplitude versus the relative spectral energy.

(3) (a) The input plane with disks used for the simulation Correlation peaks intensity plots for the two disks using a:(b) Matched filter, (c) Phase-only filter, (d) IEJTC at m = 10^{-2}, (e) IEJTC at m=10^{1}, (f) IEJTC at m=10^{3}

(4) (a) The input plane with tanks used for the simulation Correlation peaks intensity plots for the two tanks using a: (b) Matched filter, (c) Phase-only filter, (d) IEJTC at m = 10^{-2}, (e) IEJTC at m = 10^{1}, (f) IEJTC at m = 10^{3}

2.1.6 References:

(1) J. Khoury, M. Cronin-Golomb, P. Gianino, and C. Woods, J. Opt. Soc. Am. B, 11, 11 (1994).

(2) J. Khoury, J. Kane, G. Asimellis, M. Cronin-Golomb, and C. Woods, Appl. Opt., 33, 35 (1994).

(3) A. A. Jamberdino, J. E. Ludman, H. J. Caulfield, C. L. Woods, D. Freeman, and C. Ward, JOSA, 72, 1720 (1982).

(4) Y. Shi, D. Psaltis, A. Marrakchi, and A. R. Tanguay, Jr., Appl. Opt., 22, 3665 (1983).

(5) D. O. North, Proc. IEEE, 51, 1016 (1963).

(6) K. F. Fielding, and J. L. Horner, Proc. SPIE, 1151, 130 (1989).

(7) M. Cronin-Golomb, B. Fischer, J.O. White, and A. Yariv, IEEE J. Quantum Electron., QE 26, 484 (1989).

(8) A. Marrakchi, A. R. Tanguay, Jr., J. Yu, and D. Psaltis, Opt. Engin., 24, 124-131 (1985).

(9) PNR is defined by Eq. (8) of: J. L. Horner, Appl. Opt., 31, 2, 165-166, (1992).

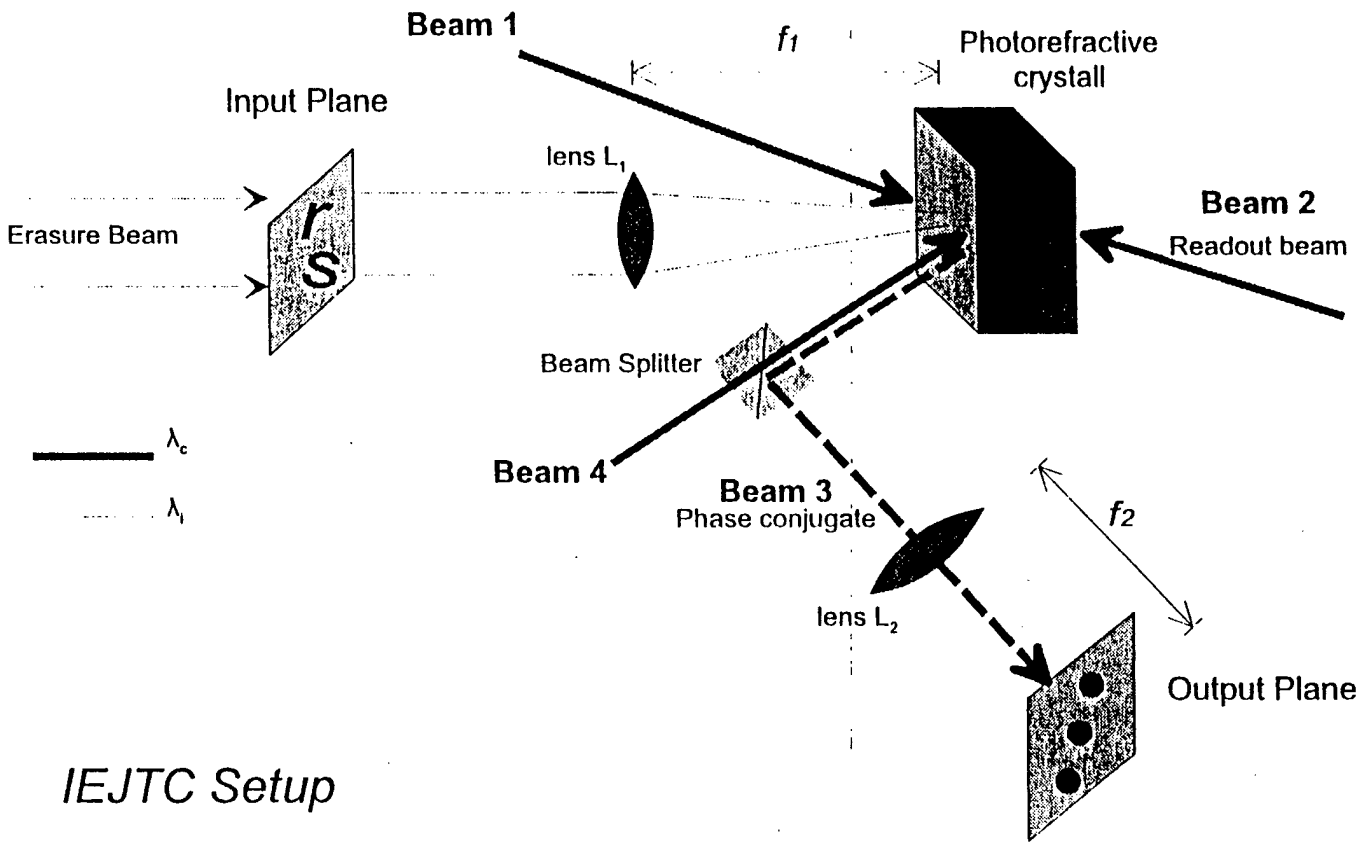
Beam 1
f_1
Photorefractive crystall
Input Plane
lens L_1
Erasure Beam
r
s
Beam 2
Readout beam
Beam Splitter
λ_c
λ_r
Beam 4
Beam 3
Phase conjugate
f_2
lens L_2
Output Plane

IEJTC Setup

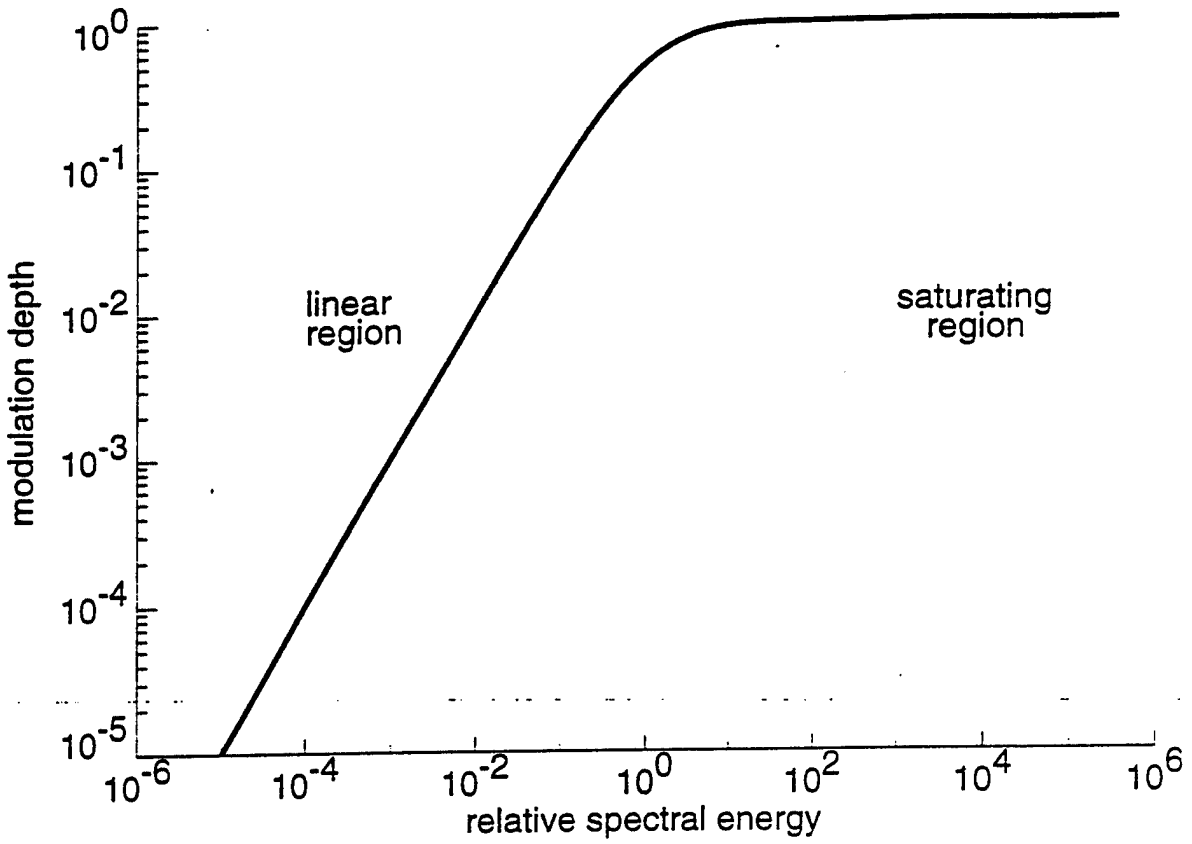
10^0
10^{-1}
10^{-2}
10^{-3}
10^{-4}
10^{-5}
modulation depth
linear region
saturating region
10^{-6}
10^{-4}
10^{-2}
10^0
10^2
10^4
10^6
relative spectral energy

Fig. 2

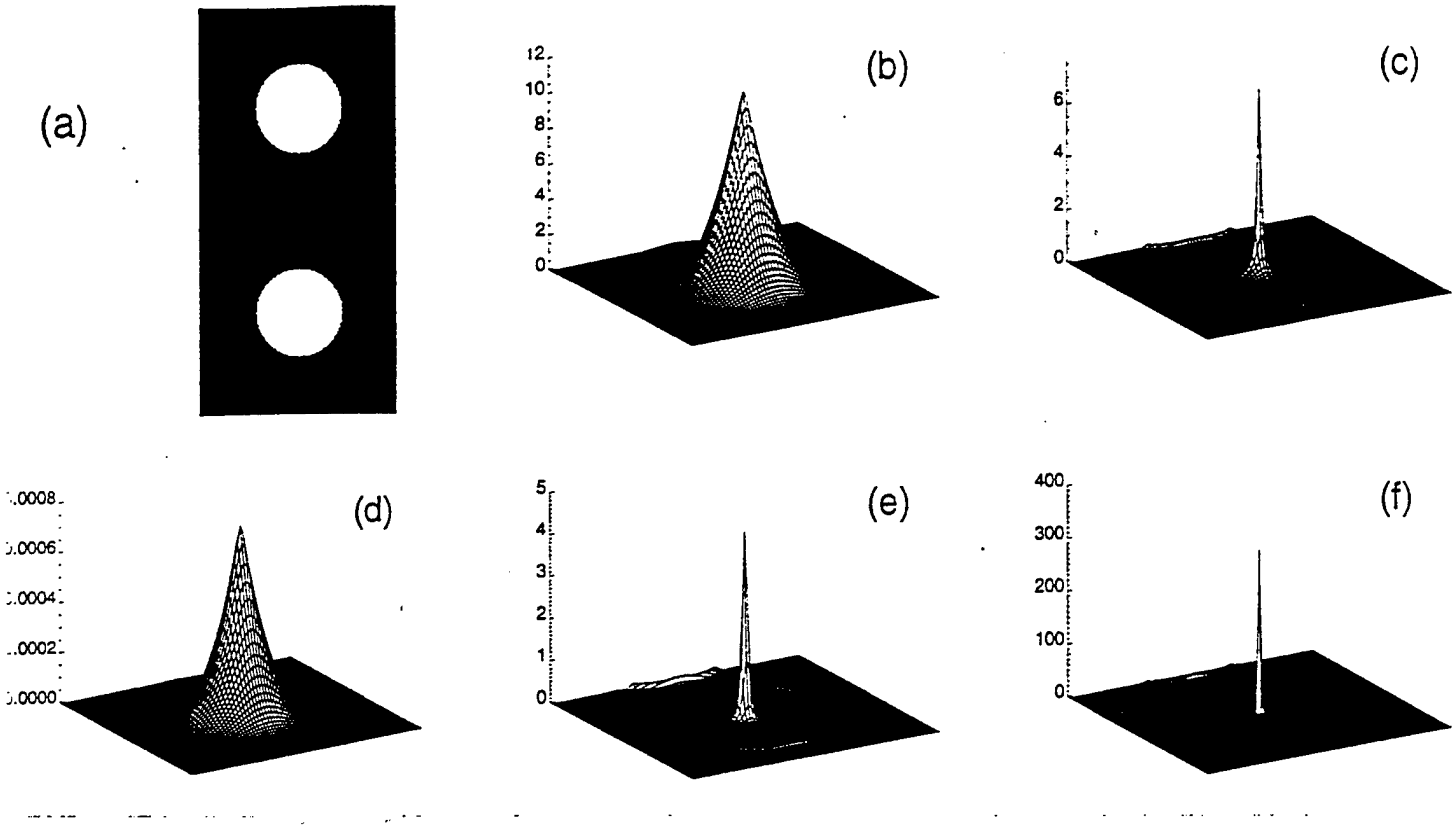
(a)
(b)
12
10
8
6
4
2
0
(c)
6
4
2
0
.0008
.0006
.0004
.0002
.0000
(d)
(e)
5
4
3
2
1
0
(f)
400
300
200
100
0

Fig. 3

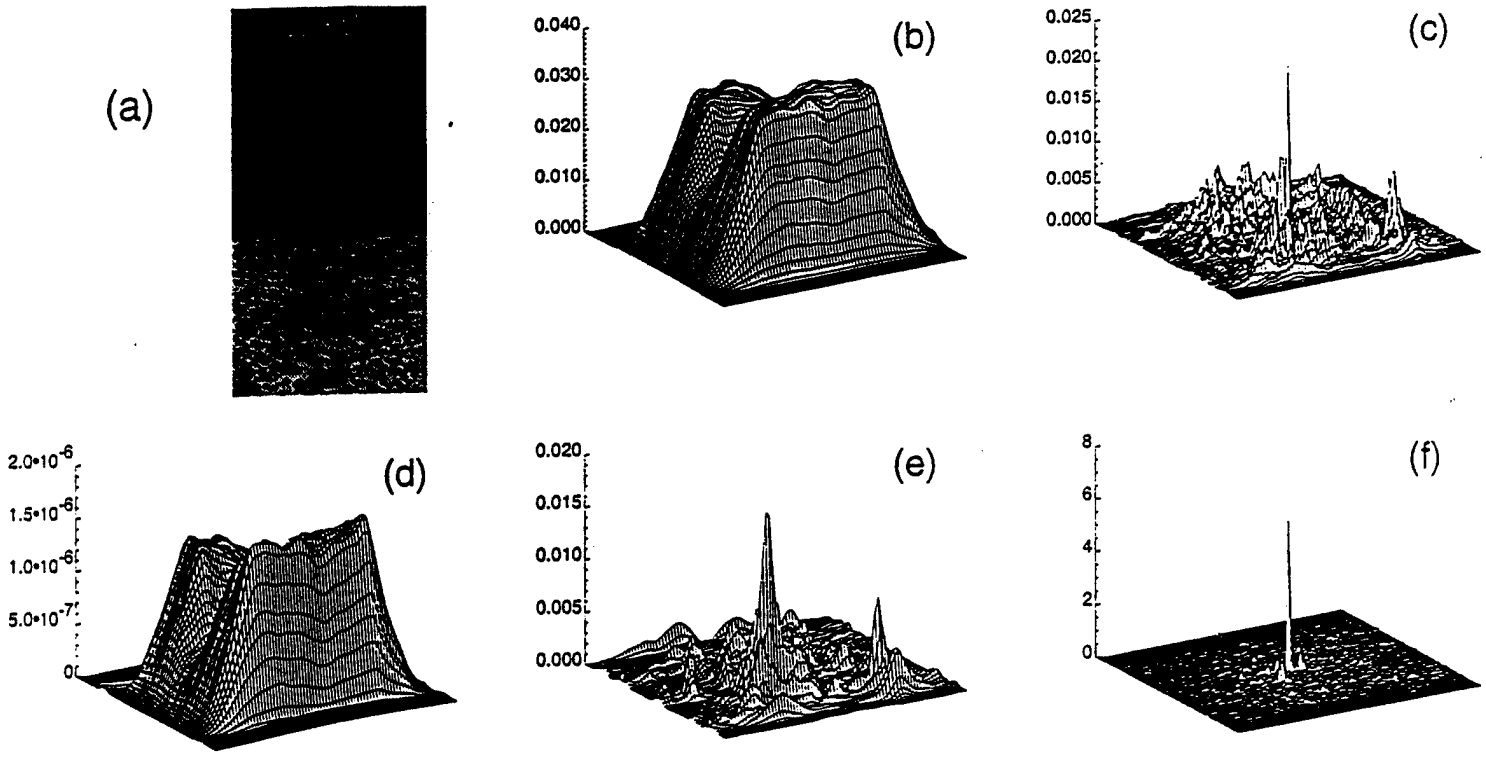
(a)
(b)
0.040
0.030
0.020
0.010
0.000
(c)
0.025
0.020
0.015
0.010
0.005
0.000
(d)
2.0•10-6
1.5•10-6
1.0•10-6
5.0•10-7
0
(e)
0.020
0.015
0.010
0.005
0.000
(f)
8
6
4
2
0

Fig. 4

Chapter 3

Speckle Velocimeter

3.1.0 Abstract

In this chapter we propose a speckle velocimeter which is based on using a real-time hologram in four wave mixing as a time-integrative correlator. The theory of the speckle velocimeter has been developed for the time correlation between the far-field spectrum of light scattered from the diffuser and reference wave which is doppler shifted. Our theoretical derivation shows that the output from the time-integrative correlator is proportional to the square of the velocity. The proportionality factor is dependent on three factors: (a) a complicated function of the ratio between the surface roughness and the granularity; (b) the input beam ratios; and (c) the coupling coefficient of the photorefractive media.

3.2.1 INTRODUCTION

Speckle metrology (1) and velocimetry(2-4) have been applied to numerous applications in solid and fluid mechanics. These applications range from fluid-flow research, wind tunnel testing, flow control system and combustion. There is substantial literature describing various designs, theory and operational mechanisms of various speckle velocity meters(2-8) . However, the operational mechanism of these devices can be divided into two main categories. The first category is the interferometric (9,10,11) and the second is time correlation (6,7,8). The interferometric techniques have been applied by using double exposure techniques in either a real-time hologram or a photographic(9,10,11) film or by using an array of CCD (13) detectors.

The implementation using photographic films is not real-time because a chemical process is required to develop the hologram. However, the implementation using real-time holography or a CCD array is also not real-time because it still requires substantial digital processing which compromises the advantages sought by the optical signal processing.

The other approach which measures the autocorrelation function assumes that when a coherent light illuminates a moving rough surface the generated speckle pattern fluctuates accordingly. Therefore, if a photodetector records the variation of the light intensity, that should be a measure of the velocity of the

diffuser. The simplest method to determine the velocity is to measure the autocorrelation function of the speckle pattern. The measurement of the autocorrelation function has been used to determine the speed of linearly moving and rotating objects. The drawback is that, these systems measure the fluctuation only at one point in space which does not give enough sampling points. The second drawback is that these systems are is not immune to background vibrational noise. To overcome this problem, Moran, et al., described a new way to measure the correlation function using a phase-locked speckle electronic pattern (6,7).

The new system used an array of CCD detectors in order to measure the fluctuation over the whole field. The background noise was isolated by using phase-lock homodyne or heterodyne detection , in order to demodulate the fluctuation in the speckle pattern from the background noise. The reference signal was generated electronically.

This system has demonstrated the ability to perform with high sensitivity even the presence of vibrational background noise whose level would destroy the performance of conventional non-isolated speckle velocimeters.

Recently, we demonstrated the first optical lock-in amplifier which operates on the principle of time correlation using four-wave mixing in real-time holography(13,14,15). This optical lock-in amplifier has been used by Lockheed for analysis of vibration (16).

In manner similar to Moran, et al. our lock-in amplifier can be used as a speckle velocimeter. The advantage here is that the new design is simpler to implement and more cost effective by using a large plate of photorefractive polymers (17). Further more our proposed device gives a direct measurement of the speed without any further processing.

In this chapter we will present (a) the theory of light scattered out of a diffuser moving with longitudinal motion,(b) the description of the device, (c) the theory of the two-dimensional time correlation detector using photorefractive media and (d) the time correlation between speckle from a diffuser moving with longitudinal motion and doppler-shifted light.

3.2.2 SPECTRUM OF LIGHT SCATTERED FROM A LONGITUDINALLY MOVING DIFFUSER

Various theories in the past have been developed to describe the far field spectrum of light scattered from a diffuser. The theories have already been developed for transverse (18), longitudinal(19) and rotational motions of diffusers (20,21). Since we are going to develop the theory of speckle velocimeter of diffuser with a transverse motion, therefore we are going to represent the theory of light scattered from a moving diffuser with transverse motion (18).

The far field spectrum S^{∞} of light scattered from a longitudinally moving diffuser of aperture A is given by:

$$S^{\infty}(\Omega', ru') = \frac{A}{2\pi}\left(\frac{\cos\theta}{cr}\right)^2 \Omega'^2 \overline{C_D}(\Omega'', K)\, S_i(\Omega'')$$

where C_D is the two-dimensional spatial Fourier transform of the diffuser correlation function. $S_i(\Omega'')$ is the spectrum of the incident light on the diffuser, r is the distance between the aperture and the observation point,c isthe speed of light, θ is the angle that the direction u' makes with the z axis. u'per is the projection , considered to be a two-dimensional vector unit u'on the aperture A. Ω',Ω'' are the frequencies of the light scattered by and incident on the diffuser, respectively. $\Omega'$and Ω'' are related by

the following formula:

$$\Omega''=\Omega'(1-\beta u')=\Omega'(1-\beta\cos\phi)$$

in which β=v/c, and ϕ is the angle between u and v. See Fig 1(a) and 1(b) for further illustrations

The Fourier transform of the correlation function is given by:

$$\overline{C_D}(\Omega,f)=\frac{1}{2\pi}\int C_D(\Omega,\varrho')\exp(-if.\varrho')\,d^2\varrho'$$

where ρ is the vectorial difference between two arbitrary points in the diffuser, while the diffuser correlation function is given by

$$C_D(\Omega:\varrho)=\exp(\eta(\Omega)(1-g(\varrho))$$

g is the normalized correlation function of the diffuser height and is defined as:

$$g(\varrho)=g(\varrho_1-\varrho 2)=\frac{<h(\varrho_1)h(\varrho_2)>-<h(\varrho_1><\varrho_2)>}{\sigma_h^2}$$

σ_h is the variance of the plate thickness and is given as:

$$\sigma_h^2 = \langle [h(\varrho) - \langle h(\varrho) \rangle]^2$$

For a diffuser which obeys the Poisson distribution(22) (i.e. in a diffuser of width W and cell size l_c), the probability of having T cells within the interval W is given by:

$$P_T = (W/l_c)^T \exp(-W/l_c) \qquad T=0,1,2.....$$
$$0 \qquad otherwise$$

The normalized correlation function for a binary or multilevel diffuser with a Poisson distribution is given by:

$$g(\varrho) = 1 - \frac{\varrho}{l_c} \quad when \quad \varrho \le l_c$$
$$0 \quad when \quad \varrho > l_c$$

For a ground glass diffuser with Poisson distribution, the normalized correlation function is given by:

$$g(\varrho) = \exp -\varrho/l_c = 1 - \frac{\varrho^2}{l_c^2} + \frac{\varrho^4}{l_c^4} - \frac{\varrho^6}{l_c^6} + ...$$

Substituting Eq. (8) in Eq. (4) yields:

$$C_D(\Omega, \varrho) = \exp[-\frac{\Omega}{C}(n(\Omega) - 1)\frac{\sigma_h}{l_c}\varrho]^2 =$$
$$\exp -\frac{2\pi}{\lambda}[(n(\Omega) - 1)\frac{\sigma_h}{l_c}]^2$$

For a ground glass diffuser the additional terms in Eq. (9) can be included. By calculation of the Fourier transform of Eq. 3 and substitution into Eq.(1) yields the following result:

$$S^{**}(\Omega', ru') = \frac{N}{n(\Omega'')-1} S_i(\Omega'') \exp - \frac{[l_c \sin\theta]^2}{2[\sigma_h (n_{(\Omega'')}-1)(1-\beta u_\perp')]^2}$$

where N is a frequency-independent normalization factor, defined as:

$$N = \frac{A l_D^2 \cos^2\theta}{[2\pi r \sigma_h (1-\beta u_\perp')]^2}$$

The interesting feature of Eq.(11) is that the Doppler shift of the scattered light is mostly dependent on v/c cos ϕ, where ϕ is the angle between uper and v . The weighting factor of the Doppler shift (or the power spectrum) at a certain angle θ is dependent mainly on the ratio between l_c and σ_h. The dependence in the previous form looks to be very logical for the following reason. When light is scattered out of a diffuser, the light can be scattred into the far field in any angle between θ=0 up to θ=90. According to the doppler shift theory, the frequency of the scattered light at a certain position should be dependent only on the speed of the source relative to the point of observation (i.e.

on θ, ϕ and v). The dependence of the power spectra on l_c and σ_h because the light scattering dependent only in the diffuser cell charactaristic even further on the ratio between l_d and σ_h. This because a larger σh will make the variation in the phase of the scattered light faster, while a larger lc deminishaes the variation in the phase of the scattered light.

3.2.3 THE TIME INTEGRATIVE CORRELATOR

Consider three beams of the same wavelength A_1, A_2, and A_4 intersecting within a photorefractive medium, as shown in Fig (2). A_1 and A_4 are coherent so they combine to induce a hologram within the material; while A_2 are coherent within themselves, but not with A_1 and A_4. Mathematically the amplitudes are

$$A_1 = E_1(t)\exp[i(k_1 r - \omega_1 t)]$$
$$A_2 = E_2(t)\exp[i(k_2 r - \omega_2 t)]$$
$$A_4 = E_4(t)\exp[i(k_4 r - \omega_4 t)]$$

In the steady state case (i.e beams A_1 and A_4 not varying in time) a hologram is written and a phase conjugate is generated. This phase conjugation is counter propagating with respect to beam A_4. Treatment of the time varying input necessitates the solution of the photorefractive space charge field in the dynamic regime. For the sake of simplicity we will assume that the total intensity of the beam incident on the crystal is constant (i.e any amplitude variation in the input beams is considered small compared to the summation of the intensities of all the beams). The development of the space charge field (E_{sc}) within the crystal is described by

$$\frac{\partial E_{sc}}{\partial t} + \frac{E_{sc}}{\tau} = \frac{\gamma}{\tau}\frac{A_1 A_4^*}{I_0}$$

where τ is the response time of the grating formation , γ is the coupling coefficient of the material, and I_o is the total intensity incident on the crystal. Equation (14) assumes that the readout beam is sufficiently weak so that it does not effect the grating. The general solution of Eq. (14) is

$$E_{sc}=Ce^{\frac{t}{\tau}}+e^{-\frac{t}{\tau}}\int_0^{\infty}\frac{\gamma A_1(t)A_4^*(t)}{\tau}dt$$

Equation (15) can be treated by assuming that $A_1(t)$ and $A_4(t)$ are signals with Fourier transforms such that

$$E_{sc}=Ce^{\frac{t}{\tau}}+e^{-\frac{t}{\tau}}\int_0^{\infty}\frac{\gamma A_1(t)A_4^*(t)}{\tau}dt$$

Equation (16) can be treated by assuming that $A_1(t)$ and $A_4(t)$ are signals with Fourier transforms such that

$$A_1(t)=\int_{-\infty}^{\infty}S_1(\omega')\exp(-i\omega' t)\,d\omega'$$

$$A_4(t)=\int_{-\infty}^{\infty}S_4(\omega'')\exp(-i\omega'' t)\,d\omega''$$

Substituting Eq. (17) into Eq. (16) yields

$$E_{sc}(t) = \frac{\gamma}{I_0 \tau} \int_{-\infty}^{\infty} \int_{-\infty}^{\infty} \frac{S_1(\omega') S_4^*(\omega'')}{-(\omega' - \omega'') + \frac{1}{\tau}} x$$
$$\exp[-i(\omega' - \omega'')t] \, d\omega' d\omega''$$

In the diffusion limit τ is a real number. With a dc electric field applied to the crystal, τ becomes complex:

$$\frac{1}{\tau} = \frac{1}{\tau_1} + i\omega_g$$

This yields

$$E_{sc} = [(\gamma / I_0)(1/\tau_1 + i\omega_g)] \int_{-\infty}^{\infty} \int_{-\infty}^{\infty} \frac{S_1(\omega') S_4(\omega'')}{-i(\omega' - \omega'' + \omega_g) + \frac{1}{\tau_1}}$$
$$\exp[-i(\omega' - \omega'' + \omega_g)\frac{t}{\tau}] \, d\omega' \, d\omega''$$

3.2.4 TIME CORRELATION WITH SPECKLE

Figure 3 shows a schematic diagram of the speckle velocimeter using a photorefractive medium. A laser beam incident on the

acousto-optic modulator Is divided into two beams: A_1 and A_4. Beam A_4 is the deflected doppler-shifted component of the beam, while beam A_1 is the transmitted component. Beam A_4 passes through a moving diffuser thereby generating a nonstationary speckle pattern with doppler shift.

The light from the two beams is combined together in a photorefractive crystal. The recombined light can write a grating as long as the doppler shift in beam A_1 is near the doppler shift of some of the light scattered by the diffuser. Beam A_2 is a read-out beam of the grating. The scattered light of the grating is directed by the beam splitter into the detector, which can also be a CCD array. The measured light is analyzed to detect the velocity of the diffuser.

Let us consider that the reference beam is given by:

$$A_1(t) = A_1 e^{(j\omega_1 t)}$$

or, in the spectrum domain it is given by

$$S_1 = (\omega') = A_1 \delta(\omega' - \omega_1)$$

For the sake of simplicity, it is possible to assume that there is no dispersion in the index of refraction of the diffuser. Accordingly, let us assume that $n(\Omega'') = n_o$ and that the incident

light into the diffuser is monochromatic at the frequency Ω", i.e.,

$$A_4(\omega'') = \delta(\omega''-\Omega'')$$

By replacing Ω" by ω"-Ω" and substituting Eqs (11), Eq (23) and (24) in to Eq. (2), it is possible to show that.

$$E_{sc} = \frac{A_1 A_4 N}{[n_o-1]^2} \exp\left[-\frac{(l_c \sin\theta)^2}{2[(\sigma_h(n_o-1)(1-\beta u_\perp)]^2}\right] x\left[\frac{\gamma}{I_0}\left(\frac{1}{\tau_1}+i\omega_g\right)\right] \frac{e^{j(\omega_1-\Omega'')}}{-j(\omega_1-\Omega''+\omega_g)+\frac{1}{\tau_1}}$$

Let us define a new parameter, which we shall call the diffuser cell characteristic parameter (DCCP), a_d. This parameter is defined as:

$$a_d = \frac{l_d}{\sigma_d(n_o-1)}$$

Substituting (DCCP) in Eq. (25) yields the following format:

The integrated intensity of the output is given by:

$$E_{sc}=\frac{\gamma A_1 A_4}{I_o}\frac{A}{(2\pi r)^2}$$
$$a_d^2\left[\frac{\cos\theta}{(1-\beta\cos\phi}\right]^2\exp\left(-\frac{a_d}{2}\frac{\sin^2\theta}{(1-\beta\cos\phi)^2}\right)$$
$$\left(\frac{1}{\tau_1}+i\omega_j\right)\frac{e^{i(\omega_1-\Omega'')}}{-i(\omega_1-\Omega''+\omega_g)+\frac{1}{\tau_1}}$$

$$I_{out}=\int_0^{2\pi}\int_{-\pi}^{\pi}|E_{sc}|^2|A_4|^2 l^2 d\theta\ d\phi$$

This integral is very difficult to evaluate analytically. However, it is still possible to do some approximations in order to evaluate it. We can consider that the second term in Eq. (27) is dependent on θ, because the value of v/c is always very small, While the third term in the same equation can be expanded into a Taylor series because in the lock-in approximation:

$$|(\omega_1-\Omega''+\omega_g)\tau|<1$$

For evaluating the whole output, it is necessary to evaluate the integration of the squares of the second and third terms of Eq. (27).

By neglecting the dependence on Φ in the square of the integral of Eq. (27), then this integral can be approximated as:

While the integration of the square of the third term for the first

$$H(a_d) = \int_{-\pi}^{\pi} a_d^2 \cos^4\theta \exp(-a_d \sin^2\theta)\, d\theta =$$

two orders of the Taylor expansion is given by:

$$\int_0^{2\pi} \left| \left(\frac{1}{\tau_1} + i\omega_g\right) \frac{e^{i(\omega_1 - \Omega'')}}{-i(\omega_1 - \Omega'' + \omega_g) + \frac{1}{\tau_1}} \right|^2 d\phi =$$

$$[1+(\omega_g\tau)^2] \int_0^{2\pi} \frac{d\phi}{1+|\omega_1 - \Omega'' + \omega_g|^2}$$

$$[1+(\omega_g\tau)]^2 \int_0^{2\pi} (1 - |(\omega_1 - \Omega'' + \omega_g)\tau_1|^2 d\phi +$$

$$|(\omega_1 - \Omega'' + \omega_g)\tau_1|^4 d\phi \ldots$$

Let us assume that the frequency of the light scattered off the acousto-optic transducer is given by:

$$\omega_1 = \omega_o(1-\beta_1) = \omega_o\left(1 - \frac{V_1}{C}\right)$$

where v_1 is the speed of the propagation of the sound in the acousto-optic modulator, ω_o is the frequency of the laser source which is also equal to Ω'' (i.e $\omega_o = \Omega''$). The integration of first term in the series in Eq. (32) is equal to:

$$[1+(\omega_g\tau)^2]\,[\pi(\omega_o\beta)^2 + 2\pi(\omega_o\beta_1 - \omega_g)^2]$$

The integration of the second term in the series of Eq. (32),

includes terms to the power four in $\beta 1$ and β and cross terms to the power two in $\beta\beta 1$, therefore, these latter terms are neglible compared to the first term.

According to the integral evaluation, the total intensity at the output is given by the following formula:

$$I_{out}=\frac{\Gamma I_1 I_4 I_2}{I_o}\left(\frac{A}{2\pi r}\right) g(a_d)\,[1+(\omega_g\tau_1)^2]\,[\pi(\omega_o\beta^2)+2\pi(\omega_o\beta_1-\omega_g)^2]$$

where Γ is the coupling coefficient in the intensity. It is evident from this equation that the integrated intensity of the output is dependent on the square of the speed. This fact makes the current device very easy to implement experimentally in the sense that there is no need for extra processing of the output. A simple electronic circuit which takes the square root of the current should gave a direct measurement of the speed.

So far, we have developed the theory of speckle velocimetry based on the far field spectrum from a moving diffuser.However, the current theory should be valid for other applications in fluid mechanics and biomedical engineering. The only difference will be in the term $H(a_d)$. This factor should be more characteristic for the speckle pattern which is scattered out of the diffuser, and would have to be recalculated for each specific problem.

3.2.5 Experimental Results.

In the past we performed some initial experiments which justifies the concept of speckle velocimetry using the photorefractive time integrative correlator. Fig. 4 shows the experimental arrangement which was used. This is essentially a standard configuration for four-wave mixing modified by two PZTs. The two PZTs are driven by two separate function generators. The source was a HeNe laser operating in a multilongitudinal mode with an output power of 30 mW and wavelength λ=632.8nm. The beam was expanded to a diameter of 2mm. Beam splitter BS_1 divided the source beam into two beams: $A_{1\ the}$ reference beam and A_4 the signal beam.

The readout beam A_2 was generated by retroreflecting A_1 from mirror M_3. A lens (f=100mm) was used in beam 4 to image the input object plane to the BSO. The measured intensities of beams I_1, I_2, I_4 were 10 mW, 5mW, and 8mW, respectively. In this experiment we used a square wave modulation instead of using ramp phase modulation. We chose this kind of modulation in order to maximize the erasing tendency of the modulation in a coherent erasure technique. (This may change the results slightly, but not significantly, because higher orders of locking will not contribute that much to the total intensity at the output. For static objects under continuous flipping of the phase, the phase conjugate beam intensity was averaged to zero. However, for moving diffusers the phase conjugate was not averaged to zero; reappearing under the constraints of time

correlation detection. Figure 5(a) is the conjugate image of the diffuser. Fig 5(b) shows the results under of the erasure by a square phase modulation. When the diffuser translated in any direction, a phase conjugate image appeared as shown in Fig 6c. The irradiance of the image is very dependent on the speed of the motion. Slow motion was very faint, with increasing speed the output irradiance increased until the frequencies of the variation in the input image no longer matched the reference beam frequencies. These qualitative results prove the operational principle of speckle velocimetry. However, further quantitative work on this aspect needs to be done.

3.2.6 Conclusion:

We have presented the theory of speckle velocimetry. Our theory is based on the use of the photorefractive time-integrative correlator and diffuser which is moving with a constant speed . In our theory we found that the output intensity is proportional to the square of diffuser velocity. In contrast to many previously proposed designs, the velocity is easily extracted without the necessity for any further processing of the output. The new current theory should open the possibility of considering the use of this device in fluid mechanics problems and biomedical applications.

A priliminary experimental result which was obtained previously justifies the current theory. However, further experimental work needs to be done to understand the theory for other cases.

3.2.7 Figure Captions.

Fig. 1 (a) Illustrative scheme to determine the far field spectrum of light scattered from a diffuser. (b) Illustrative scheme to show the projection of U in the plane of motion and the angle between uper and v.

Fig. 2 A schematic diagram to illustrate the time integrative correlator with piezo-mirrors.

Fig 3. (a) A diagram of a speckle velocimeter using an acousto-optic modulator which serves as a beam splitter as well as a doppler shift device. (b) The geometrical arrangement to produce the effect of scattered light from transverse motion of diffuser from a rotating diffuser.

Fig 4. A schematic diagram of a speckle velocimeter in the imaging geometry.

Fig 5. Illustration of speckle velocimetry with transverse motion of the diffuser.(a) The phase conjugate image with a static diffuser. (b) With square phase modulation operate on PZT1. (c) The regenerated phase conjugate with transverse motion of the diffuser.

3.2.8 REFERENCES

(1) R. K. Erf, Ed. Speckle Metrology (Academic, New York , 1978)

(2) P. G. Simkins and T. D. Dudderar, J. Fluid Mech, 89, 665 (1978)

(3) S. H. Collicott and L. Hesselink, Opt. Letts. 11, 410 (1986)

(4) R. Meynart, Appl. Opt. 22, 535 (1983).

(5) R. Barakat, "Zero-crossing rate differential speckle intensity," J. Opt. Soc. Amr .A 11,671-673 (1994)

(6) S. E. Moran, Robert L. Law. P. N. Craig and W. M. Goldberg " Optically phase-locked electronic pattern interferometer," Appl Opt. 26, 475-491 (1987)

(7) S. E. Moran, R. Lugannani, P. N. Craig and R. L. Law," Optical phase-locked electronic speckle pattern interferometer system performance for vibration measurement in random displacement field," 6, 252-269 (1989).

(8) B. E. Saleh, "Speckle correlation measurement of the velocity of small rough rotating rough objects," Appl. Opt. 14, 2344-2346, (1995)

(9) S. H. Collicott and L. Hesselink, "Real-time photorefractive recording and optical processing for speckle velocimetry," Opt Letts, 43< 348-350 (1988)

(10) K. Nakagawa and T. Minemoto "Readout properties of speckle recorded in photorefractive $Bi_{12}SiO_{20}$," Appl. Opt. 17, 2386-2392 (1991)

(11) H. J. Tiziani, K. Leonnhard and J. Klenk, "Real-Time displacement and tilt analysis by a speckle technique using $Bi_{12}Si_{12}O_{20}$, 34, 327-331 (1980)

(12) Hesselink, "Handbook of flow visualization" (Hemisphere, New York , 1988)

(12) J. Khoury, V. Ryan, C. L. Woods and M. Cronin-Golomb, "Photorefractive optical lock-in detector," Opt. Letts. 16, 1442-1444 (1991)

(13) J. Khoury, V. Ryan, M. Cronin Golomb and C. L. Woods. "Photorefractive frequency convertor and phase-sensitive detector," J. Opt. Soc.B. 10, 72-82 (1993)

(14) J. Khoury, V. Ryan, C. L. Woods and M. Cronin-Golomb, "Photorefractive time correlation motion detection ," Opt. Commune. 85, 5-9 (1991)

(15) T. Chatters and K. Telschow, Optical lock-in detection using photorefractive four-wave mixing " Report by Idaho National Engineering Laboratory, Lockheed Idaho Technologies Co. P.O.Box 1625, Idaho Falls, Idaho 83415-2209.

(17) B. L. Volodin, S. K. Meerholz, B. Kippelen, N. V. Kukhtarev and N. Peyghambarian, "Highly efficient photorefractive polymer for dynamic holography," Opt. Eng. 34, 2213 (1995)

(18) B. Cairns and E. Wolf, "Changes in the spectrum of Light scattered by a moving diffuser plate," J. Opt. Soc Am. A ,8 1922-1928 (1991).

(19) N. Takai, Sutanto and T. Asakura, "Dynamic statistical properties of laser speckle due to longitudinal motion of a diffuse object under Guassian beam illumination," J. Opt. Soc. Am , 70, 827-834 (1980).

(20) L. E. Estes, L. M. Narducci and Richard A Tuft, "Scattering of light from a rotating ground glass," J. Opt. Soc. Am. B. 61 , 1301-1306 (1971)

(21) J. H. Churnside " Speckle from a rotating diffused object," J. Opt. Soc. Am. 72, 1464-1469, (1982).

(22) E. L. Karl, J. F. Walkup, and M. O. Hagler, Correlation properties of random phase diffuser for multiplexed holography," App. Opt. 21, 1281-1290 (1982)

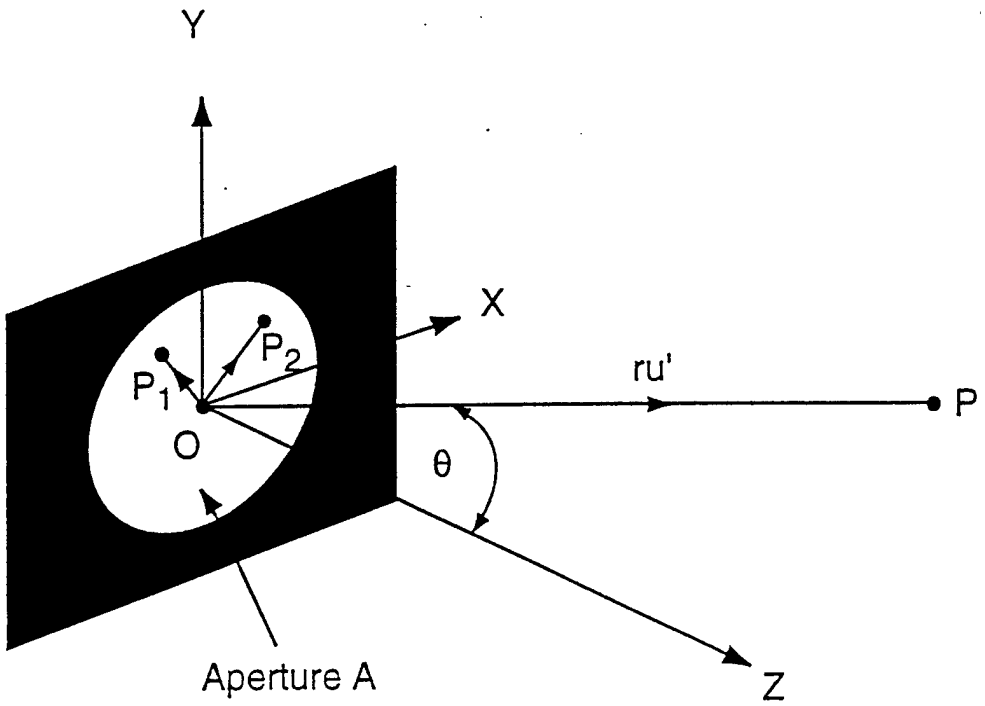
Y
X
P2
P1
O
ru'
P
θ
Aperture A
Z

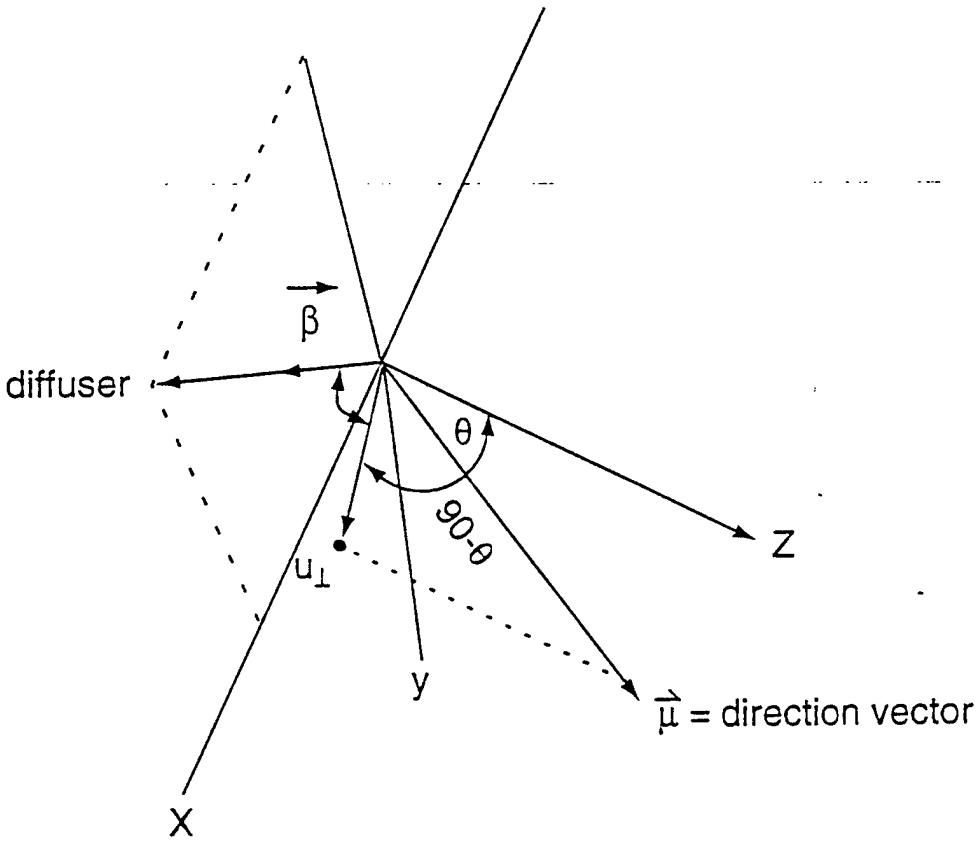
β
diffuser
θ
90-θ
Z
u⊥
y
μ = direction vector
X

Fig 1

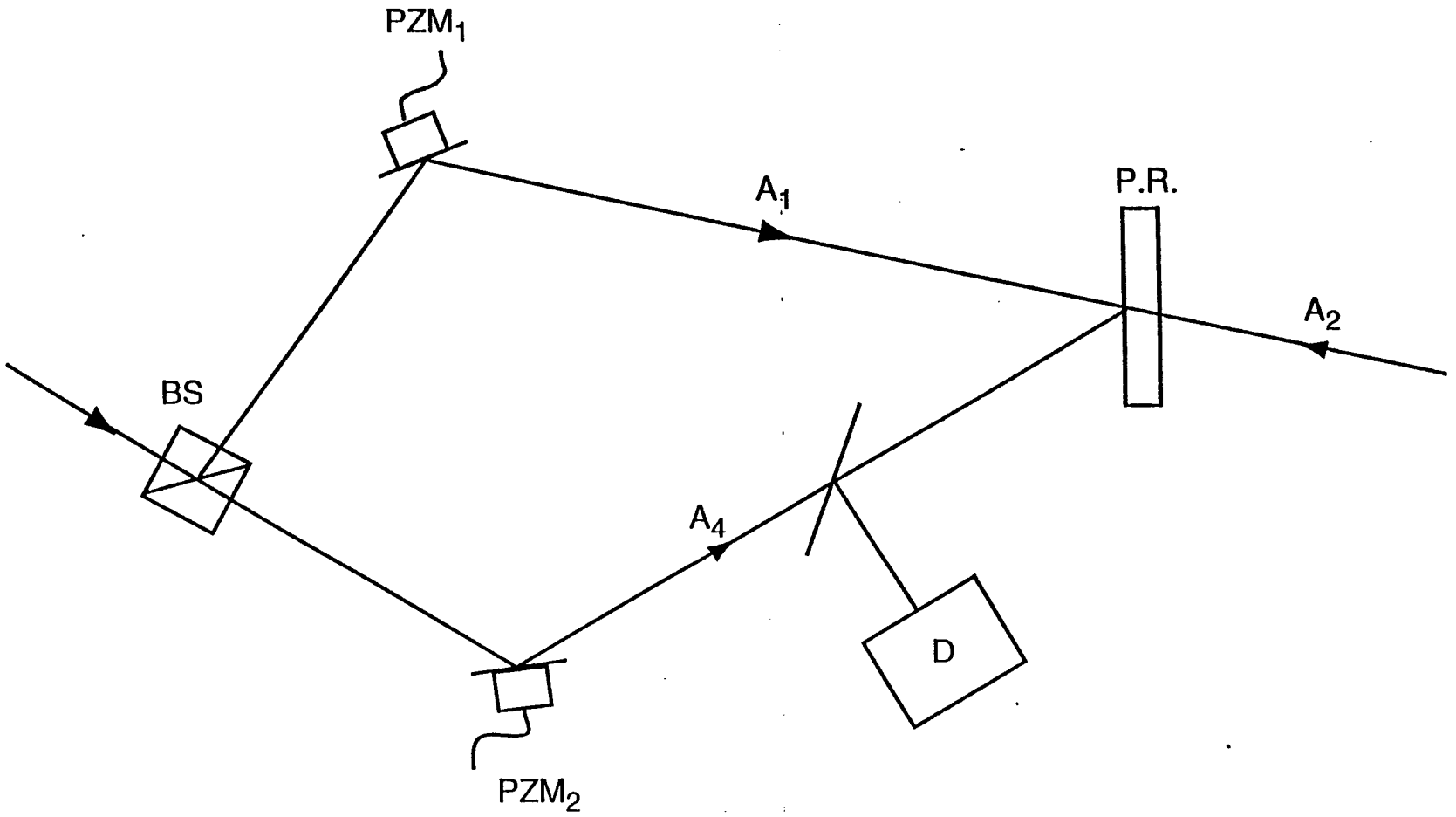
PZM1
A1
P.R.
A2
BS
A4
D
PZM2

(a)

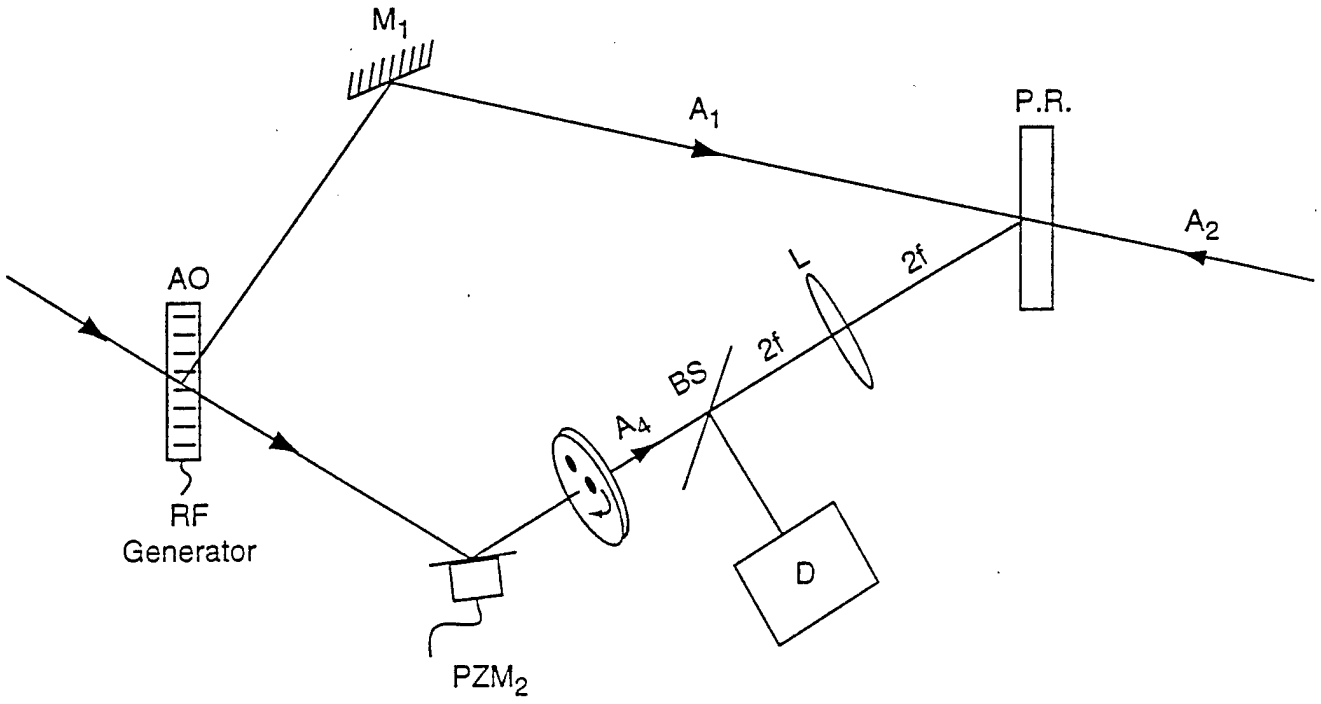

(b)

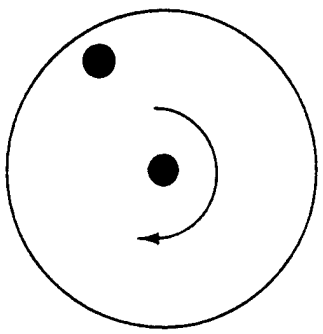

Fig. 3

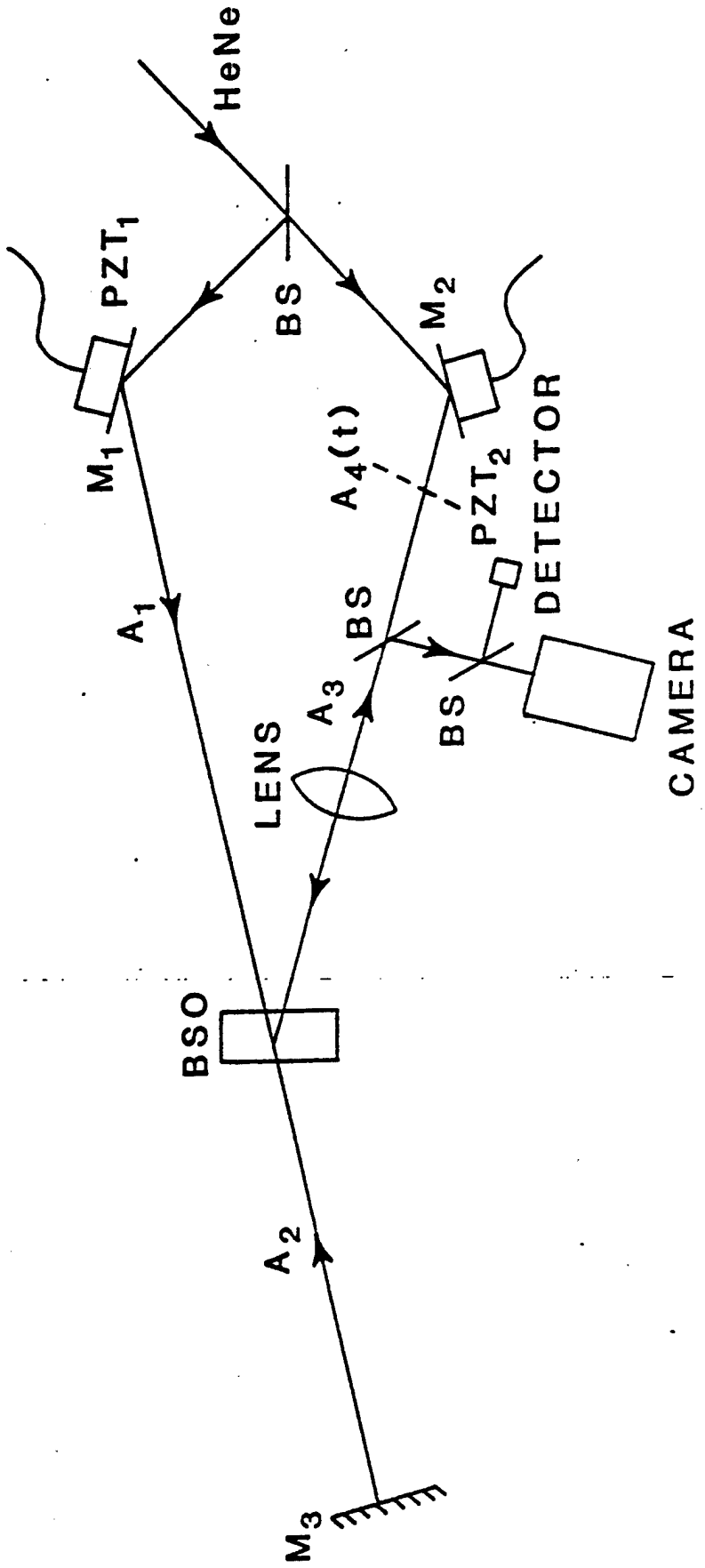
HeNe
PZT1
BS
M2
M1
A4(t)
PZT2
DETECTOR
A1
BS
A3
BS
CAMERA
LENS
BSO
A2
M3

Fig. 1

A

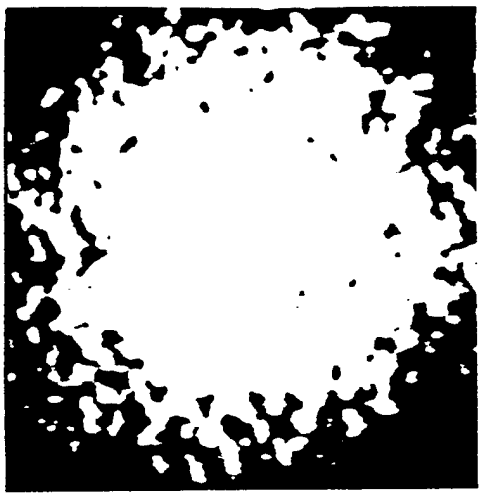

B

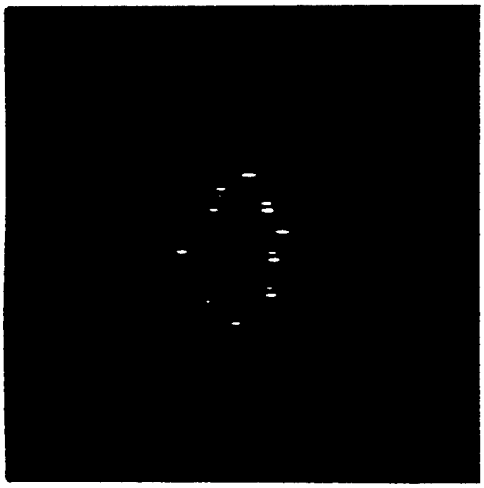

C

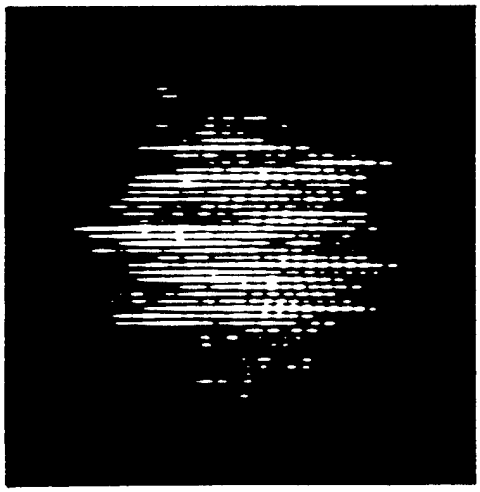

Fig. 5

Chapter 4

Homodyne and Heterodyne Imaging in a Scattering Medium

4.3.0 Abstract

In this paper we introduce two dimensional homodyne and heterodyne techniques for imaging objects in the presence of a scattering medium. These techniques are categorized into two forms according to their operational principles. The first is based on the Doppler shift difference in light scattered from objects of two different textures or an opaque object and a textured scattering medium. The second technique is based on the principle of photon density waves, but incorporates 2-d holographic detection. In both cases a two-dimensional real-time holographic phase-sensitive detector is proposed to pull the images from noise. We report the initial demonstration of pulling signals out of noise based on the Doppler shift difference. Enhancements of signal-to-noise in the order of 50 have been achieved.

4.3.1 INTRODUCTION:

Imaging through a scattering medium or imaging an object within a scattering medium is one of the most challenging problems in optical signal processing. It has significant importance in tomography and image formation in biological tissues. Various methods have been utilized to solve this. However, one of the most popular approaches is based on the principle of the first arriving light. In this technique, a time gate is used to separate the information-carrying light (the first light) from the noisy light (the subsequent light). The first realization of this scheme was demonstrated by Mantic and Duguay(1). In their specific implementation the hologram was used as a time gating processor. Since then , different time gating techniques have been used, for example, electronic holograms(2) and real-time holograms(3). Time gating has also been implemented using Kerr(4) and Raman cells(5). Further improvement in terms of signal-to-noise ratio have been achieved by adding spatial filtering techniques(6).

One drawback in the first light techniques is they require ultrafast pulses and sophisticated instrumentation for fast imaging. These facts make the above approaches expensive to implement. Therefore, we propose an alternative technique which uses a CW laser associated with homodyne and heterodyne detection.

2.3.2 Background:

In this chapter we introduce two-dimensional homodyne and heterodyne techniques for imaging objects in the presence of a scattering medium. Imaging in scattering media is important for biomedical applications (for example, imaging tumors within a healthy tissue) or transferring images within atmospheric turbulence. Our techniques are categorized into two forms according to their operational principle. The first is based on the Doppler shift difference in light scattered from objects of two different textures or an opaque object and a textured scattering medium. We also show that the basic principle of the Doppler shift difference technique and of first light are similar. The advantage is that the Doppler technique does not require a high power pulsed laser. Rather, CW lasers with modulation in the range of MHz to GHz are used. The second technique is based on the principle of photon density waves(7), but incorporates 2-d holographic detection. In both cases, a two-dimensional real time holographic phase sensitive detector is used to pull the images from noise (8,9,10,11,12). Opto-electronic devices, based on smart pixelated arrays, can also be used for this purpose.

In the first light technique a narrow pulse of light is passed through a scattering medium. The first emerging light is less severely scattered and therefore forms the best image, while the subsequent light is considered noise. The problem then reduces to extracting signal from noise by time gating.

In the Doppler difference technique, cw light is scattered by moving media of different textures (having different sized scattering centers). It is well known in statistical optics, that scattered light from a random media moving with a constant velocity will cause Doppler shifting(13,14). This is true if the motion is along, or perpendicular to, the direction of propagation of the illuminating light. An object with large scattering centers produces a relatively small angle of scatter and hence generates a small Doppler shift. In contrast, small scattering centers generate larger angles of scatter and therefore larger Doppler shifts. For example, consider an object of one texture embedded inside a medium of another texture, as in the case of a tumor in healthy tissue. Each texture will contribute different Doppler shifts. Clearly, homodyne and heterodyne techniques will be useful in separating the light scattered from each of these two textures.

Large motions of an object are not very practical. For example, if a tumor and healthy tissue are moving simultaneously, the image would be smeared. In the case of a massive object, this problem can be overcome by vibrating only the scattering medium, for example, by launching an acoustic wave. For non-sinusoidal vibrational motion of a random scattering medium, the Doppler shift spectrum shows multiple peaks at harmonics of the fundamental vibrational frequency, each with its own characteristic bandwidth depending on the statistics of the scattering medium. Objects with coarser texture will of course scatter light with less bandwidth.

This light can be separated from the other light using frequency selective detection.

In previous publications, we reported on a two-dimensional real-time holographic optical lock-in detector(8,9,10). It was also demonstrated that it is possible to detect moving texture. As in all heterodyne detection schemes, maximum detection of moving texture occurs when the center of the Doppler-shifted frequency of the scattered light from the random medium is equal to the modulation frequency of the reference optical signal(15,16,17). Nearby frequencies are also recovered and contain additional information as in all-optical baseband demodulation(18,19).

4.3.2 DEVICE DESCRIPTION:

Figure 1 shows a schematic diagram of a homodyne and heterodyne scheme for imaging within the scattering medium (A) for an object behind the scattering medium (B) for object imbedded in the scattering medium and (C) for an embedded object, but with the light itself modulated, rather than the scattering medium. Cases (A) and (B) are based on the principle of the difference in Doppler shifting while (C)is based on the principle of photon density waves, and can be extended to the case of multiple light sources with fixed phase shifts.

In all cases a two-dimensional lock-in detector is used. This

two-dimensional lock-in detector can be a real-time hologram operating with various configurations such as four-wave mixing(8,9,10), two-wave mixing(11) or a two-input version of a self-pumped phase conjugator(12). In all of these configurations, one of the input beams has the signal and the other beam has the modulated reference. Another way to implement the two-dimensional lock-in detector is to use a smart pixelated array where the homodyne and heterodyne detection can be controlled by an internal clock.

In (A) the object is set behind the scattering medium. In this case laser light passes first through the object and then through the scattering medium. An oscillation is generated by an acoustic vibrator attached to the scattering medium or some other acoustical transducer. In this case the zero Doppler-shifted light corresponds to the light which carries the information on the signal, while the Doppler shifted light corresponds to the scattered light. Therefore, homodyne detection for the non-shifted light should recover the signal. Homodyne detection on the non-Doppler-shifted light does not require a modulated reference. Thus, a simple CCD array or a time averaging hologram is sufficient for recovery of the signal from the noise. Case (B) is similar to case (A) except that the object is embedded in the scattering medium. Simultaneous vibration of an object and a scattering medium of different textures will cause each to scatter light with a different Doppler shift. Therefore, using a homodyne detection technique and proper

choice of reference frequency, it is possible to lock in on the maximum of the frequency spectrum of either the signal or the noise, with some bandwidth tolerance. (17,18,19)

The last configuration for detecting a signal in a noisy environment is based on the photon density wave experiments. In this case, the demodulated light carries the phase information of the photon density wave after it has diffracted off the object and propagated through the scattering medium. Implementation of this scheme with a single (scanning) photodiode (1-d) has been described by others [7]. The improvement described here is to perform 2-d parallel optical demodulation of the scattered light. The basic concept of photon density wave imaging relies on phase sensitive detection of an amplitude modulated laser diode. We have shown that the phase of the modulation of a laser diode beam can be directly measured using all-optical phase sensitive detection for modulation frequencies up to several GHz. This phase measurement was accomplished by varying the path length transverse by the modulated light and monitoring the optical lock-in demodulated signal [20].

4.2.4 EXPERIMENT:

Two experiments have been performed to demonstrate the principle of imaging an object behind the scattering medium. In the

first experiment a CCD camera is used, and in the second, a four wave mixer with a photorefractive BaTiO3 crystal. Both schemes are shown in Fig 2(A) and 2(B) respectively . As shown, in both cases, light reflected of the resolution chart (the object) is transmitted through nozero mean diffuser which is mounted on an acoustic vibrator, driven by sawtooth voltage. The diffuser consists of a spray-painted microscope slide. A lens focal length 30cm was used to image the resolution chart in to the camera (fig 2A). Similarly in fig. 2B, the CCD camera was replaced by four wave mixer with BaTiO3 crystal, lens l_2 was used to image the phase conjugate output into the CCD camera. The write beams (1 and 4) were extraordinary polarized, and the read out beam was ordinary polarized. These polarizations were chosen to prevent beam fanning of the crystal during the read out process, and to simplify separation of the phase conjugate and the light scattered by the crystal surface through using a polarizer.

Figure 3 shows the experimental results for imaging within a scattering medium: (A) Is the orginal image (B) the light incident on the CCD after transmission through the image and a non-moving diffusser, and (C) the light when the diffuser is vibrated at a frequency of 10Hz. The improvement in signal to noise ratio was 20. In Fig 3(B) and 3(C), the experiment is repeated using the photorefractive four-wave mixer and a vibration frequency of .... This frequency is less than the previous one because of the long time integration of the BaTio3. In this case, the SNR is improved

from 50 (Fig 3B) to (Fig 3D).

The results showed better noise removal using the photorefractive crystal. This can be attributed to two reasons. The first reason is due to amplification of the signal beam by the crystal. The second is due to rejection of the scattered light by the crystal, compared to simply averaging out the spatial content of the signal, as is the case with the camera only.

4.3.5 CONCLUSION:

In conclusion, we have proposed homodyne and heterodyne techniques for imaging in a scattering medium. The first technique is based on the principle of the Doppler shift difference of the light which is scattered from an object vs light scattered by the surroundings. We showed that the principle of Doppler shift difference, and the principle of first arriving light are similar. However, in contrast to first light, which requires ultrafast pulses, here modulated CW can be used. We also experimentally demonstrated the basic principle for a simple case of an object outside of the scattering medium. The second is an extension of the principle of photon density waves, using a two-dimensional (non-scanning) detection scheme.

Many nonlinear media can be used for the processes described. The preference is for high gain, low noise materials. The

materials which we recommend is ferroelectric photorefractive materials such as $BaTiO_3$ with Rh doping [21] in self-bending geometry [22]. This material has the largest coupling coefficient observed so far and works in the wavelength range of primary interest for biological tissues. Other materials such as thin film polymers [23] can be used with multistage amplification because one thin film is not enough. Resonant systems, such as atomic vapors [24], can also be used where high speed response at low light levels are required. In all of these geometries we can use a diverging pump beam to ensure high resolution gain [25].

4.3.6 FIGURE CAPTIONS:

Fig: 1: A schematic diagram which illustrates the principle of imaging in a scattering medium based on using two-dimensional phase sensitive detector Figures (A) and (B) are based on the principle of the Doppler shift difference: (A) for object impeded behind the scattering medium; (B) For an object embedded in the scattering medium; (C) Is based on the principle of photon density waves for an object which embedded either behind or within the scattering medium.

Fig 2: The experimental set-up used for imaging an object imbedded behind a scattering medium: (a) is based on using the CCD camera as the two-dimensional phase sensitive detector (B) base on using a photorefractive crystal as the two dimensional phase sensitive detector. In both drawings S.M. denotes a scattering medium.

Fig 3: The experimental results for imaging an object within a scattering medium: (a) The original input; (b) The results after transmission within the scattering medium; (C) The results using a CCD camera as the two-dimensional phase sensitive detector.

Fig 4: The same as in Fig 3 respectively but for the case when the photorefractive crystal has been used as the two-dimensional phase sensitive detector.

4.3.5 REFERENCES

(1) M. A. Duguary and A. Mattic,"Ultrahigh-speed photography of picosecond light pulses and echoes,"Appl. Opt. 10, 2162-2170 (1971)

(2) H. Chen, et al. ,"Two-dimensional imaging through diffusing media using 150-fs gated electronic holography techniques ," Opt. Letts. 16, 487-489 (1991)

(3) A. Rebane and J. Fienberg, "Time resolved holography," Nature 351, 378-380 (1991)

(4) L. Wang, et al. ,"Ballistic 2-D imaging through a scattering wall using an ultrafast Kerr gate," Science 253, 769-771 (1991)

(5) M. D. Duncan, et al., "Time gated imaging through scattering media using a stimulated Raman amplifier, " Opt. Lett. 16, 1868-1870 (1991)

(6) L. Wang, et al.,"Fourier-Kerr imaging in thick turbid media," Opt. Lett. 18, 241-243 (1993)

(7) M. A. O'Leary, D.A. Boas, B.Chance and A. G. Yodh, "Refraction of diffuse photon density waves," Phys. Rev. Letts. 69,2658-2661 (1992)

(8) J. Khoury, V. Ryan and C. L. Woods and M. Cronin-Golomb, "Photorefractive optical lock-in detector," Opt. Letts. 16, 1442-1444, 1991.

(9) J. Khoury, V. Ryan, C. Woods and M. Cronin-Golomb, "Photorefractive frequency convertor and phase sensitive detector," J. Opt. Soc. Am. B 10, 72-82 (1993)

(10) J. Khoury , M. Cronin-Golomb and C. L. Woods, "Photorefractive mixing of amplitude modulated signals," Opt. Letts 19, 743-745 (1994)

(11) B. Breugnot, H. Rajbenbach , M. Defour and J. P. Huignard, "Low noise photorefractive amplification and deflection of very weak signal beams," . 20, 447-449 (1995)

(12) J. Khoury, J. S. Kane and C. L. Woods "Demultiplexing and phase locking via self-pumped phase conjugate mirror", Vol 2565 Optical Information Processing," edited by B. Javidi and J. L. Horner.

(13) N. T. Sutanto and T. Asakura, "Dynamic statistical properties of laser speckle due to longitudinal motion of diffuse objects under Gaussian beam illumination", J. Opt. Soc. Am 70, 827-832 (1980)

(14) B Cairns and E. Wolf, "Change in the spectrum of light scattered by a moving diffuser plate" J. Opt. Soc. Am. A. 8. 1922-1928 (1991)

(15) J. Khoury, Ph.D Thesis, "Application of photorefractive to nonlinear information processing theory," University of Essex (1989)

(16) G. Hussain and R. W. Eason, "Velocity filtering using complementary gratings in photorefractive BSO," Opt. Commun. 86, 106 (1991)

(17) J. Khoury, V. Ryan C. L. Woods and M. Cronin-Golomb, "Photorefractive time correlation motion detection," Opt. Commun. 85, 5-9 (1991)

(18) J. Khoury, J. S. Kane, J. Kierstead, C. L. Woods and P. Hemmer, "Real-time holographic baseband frequency demodulator," Appl. Opt. 33, 2909-2916 (1994)

(19) J. Khoury, M. Cronin-Golomb and C.L. Woods, "Real-time holographic frequency division demultiplexing: Theoretical aspects," Appl. Opt., 33, 5390 (1994).

(20) J. Kane, "Gigahertz optical lock-in demultiplexer", Rome

Laboratory Report RL-TR-93-196, (Rome Laboratory, Hanscom AFB, MA (1993)

(21) M. Kaczmarek and R.W. Eason, "Very high gain single-pass two beam coupling in blue Rh:$BaTiO_3$", Opt. Lett. 20, 1850 (1995)

(22) A. Brignon, S. Breugnot, and J.P. Huignard, "Very high-gain two-wave mixing in $BaTiO_3$ with a self-bent pump beam", Opt. Lett. 20, 1689 (1995)

(23) B.L. Volodin, Sandalphon, K. Meerholz, B. Kippelen, N.V. Kukhtarev and N. Peyghambarian, "Highly efficient photorefractive polymers for dynamic holography", Opt. Eng. 34, 2213 (1995)

(24) P.R. Hemmer, D.P. Katz, J. Donoghue, M. Cronin-Golomb, M.S. Shahriar and P. Kumar, "Efficient low-intensity optical phase conjugation based on coherent population trapping in sodium", Opt. Lett. 20, 982 (1995)

(25) N.A. Vainos and M.C. Gower, "High fidelity image amplification and phase conjugation in photorefractive $Bi_{12}SiO_{20}$ ", Opt. Lett. 16, 363-365 (1991)

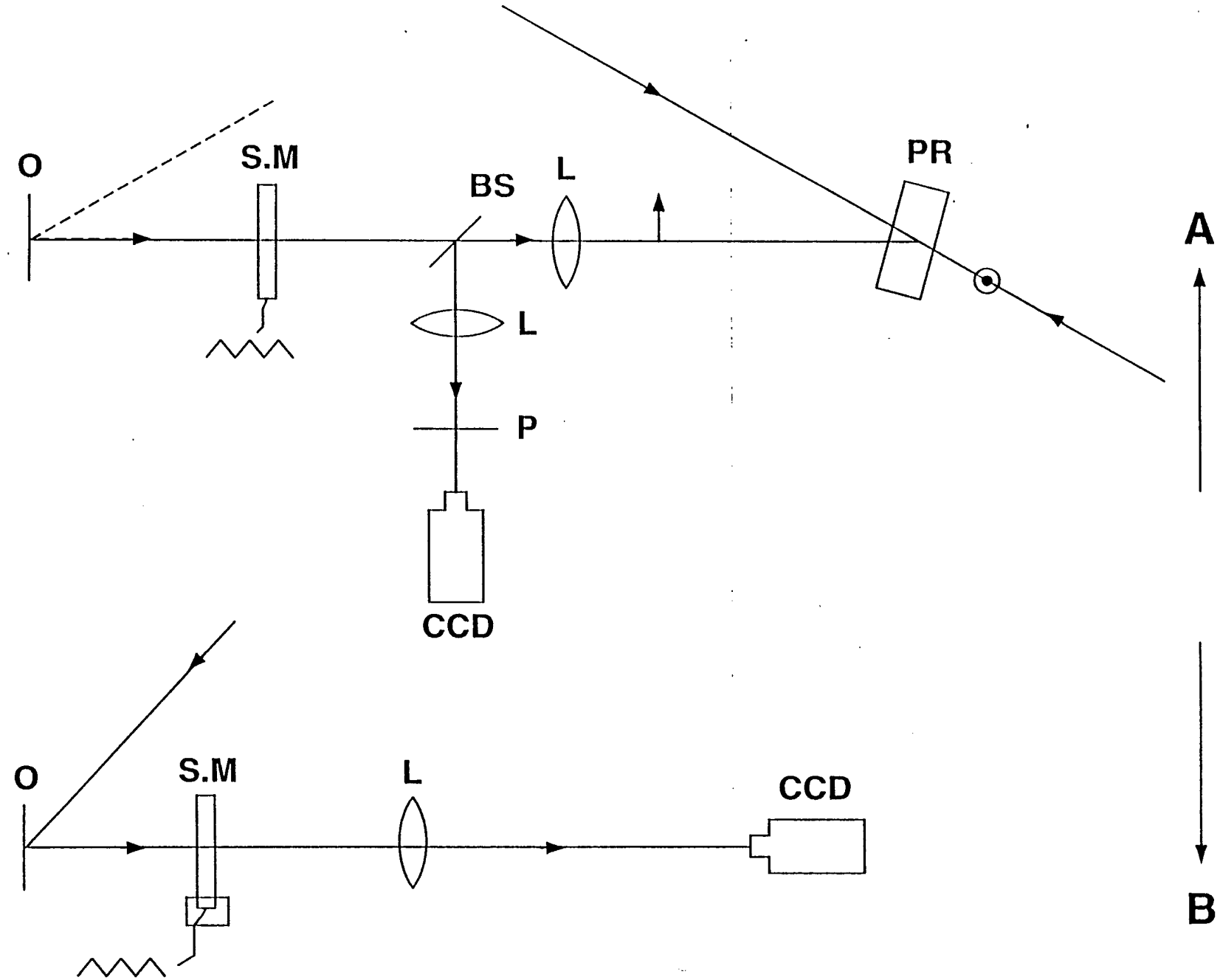
O
S.M
BS
L
PR
A
L
P
CCD
O
S.M
L
CCD
B

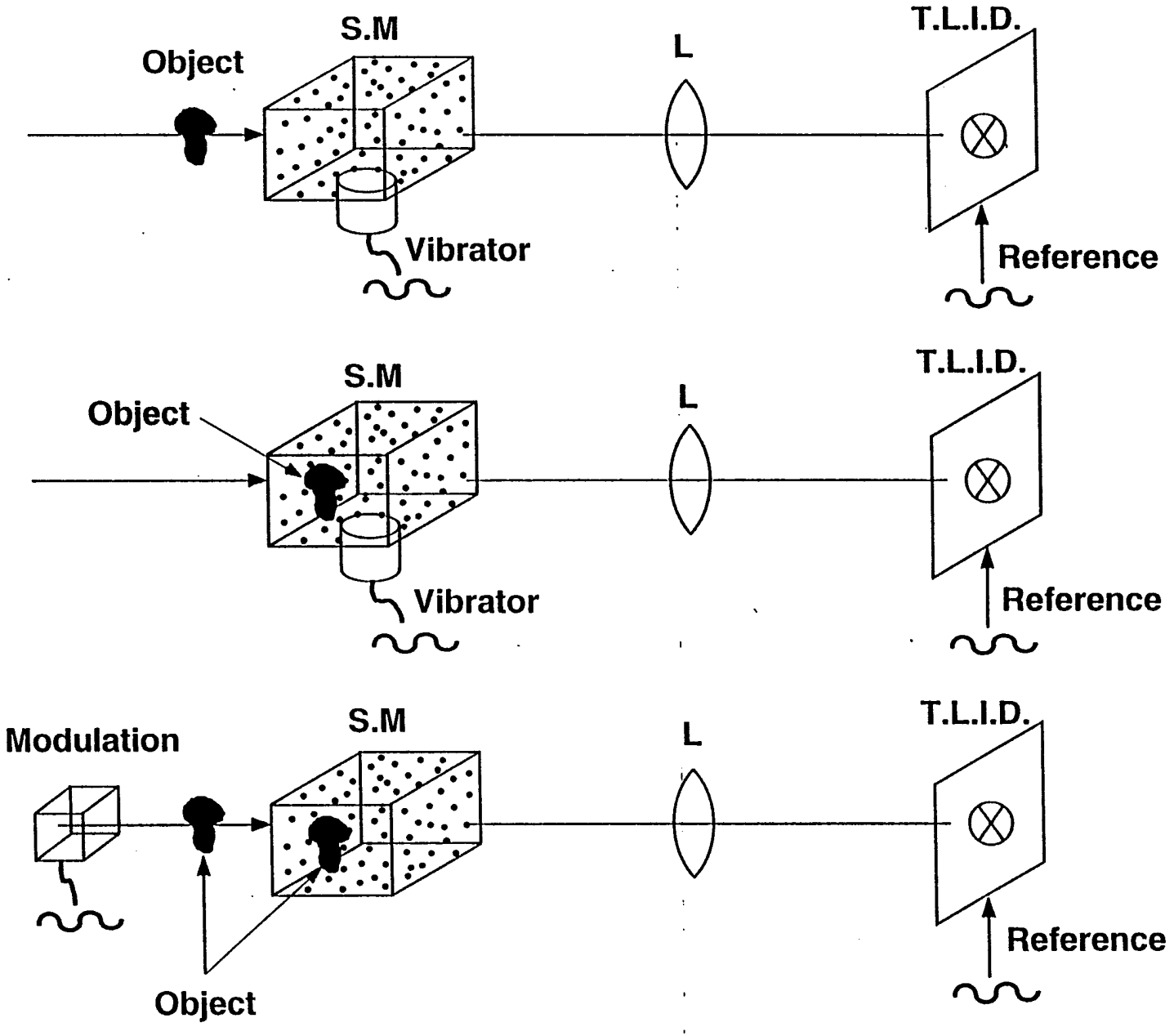
S.M
Object
L
T.L.I.D.
Vibrator
Reference
S.M
Object
L
T.L.I.D.
Vibrator
Reference
Modulation
S.M
L
T.L.I.D.
Object
Reference

Fig. 2

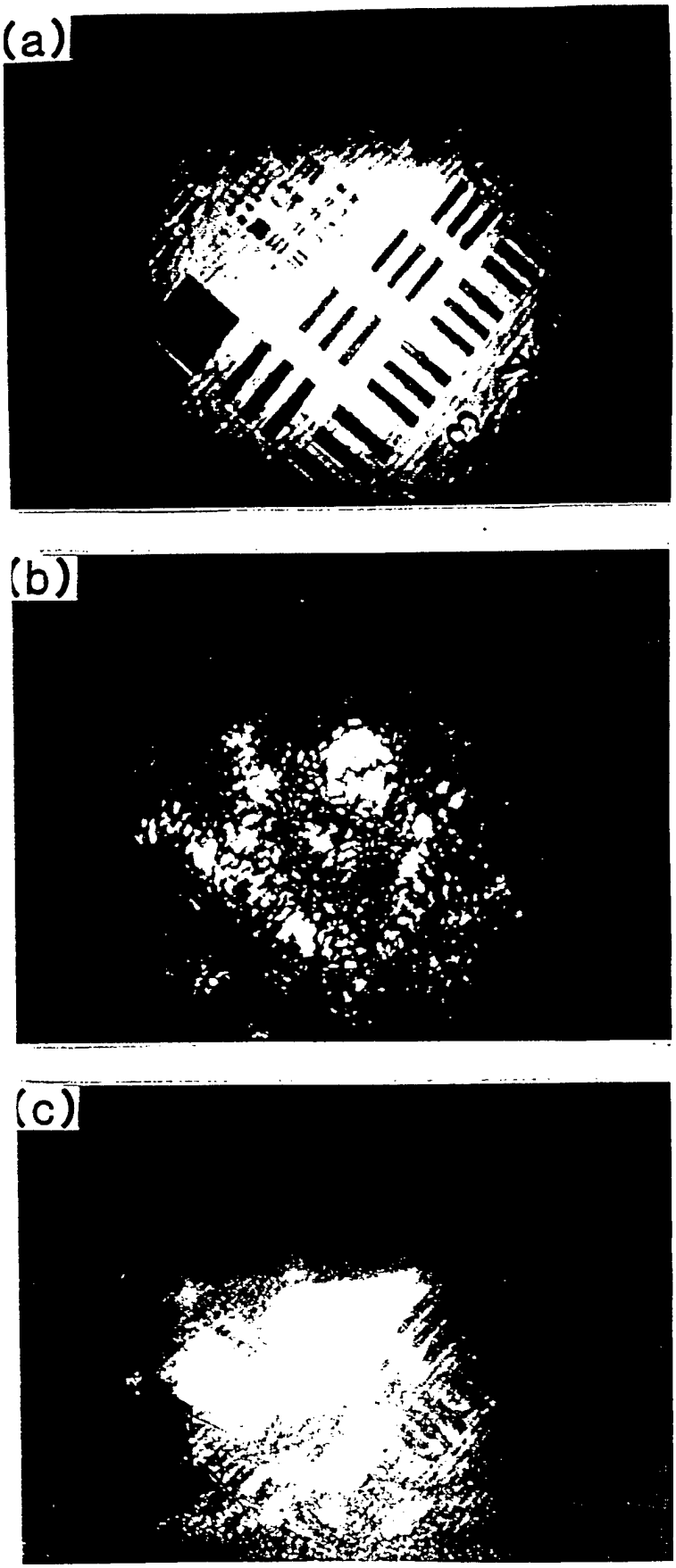

Fig. 3

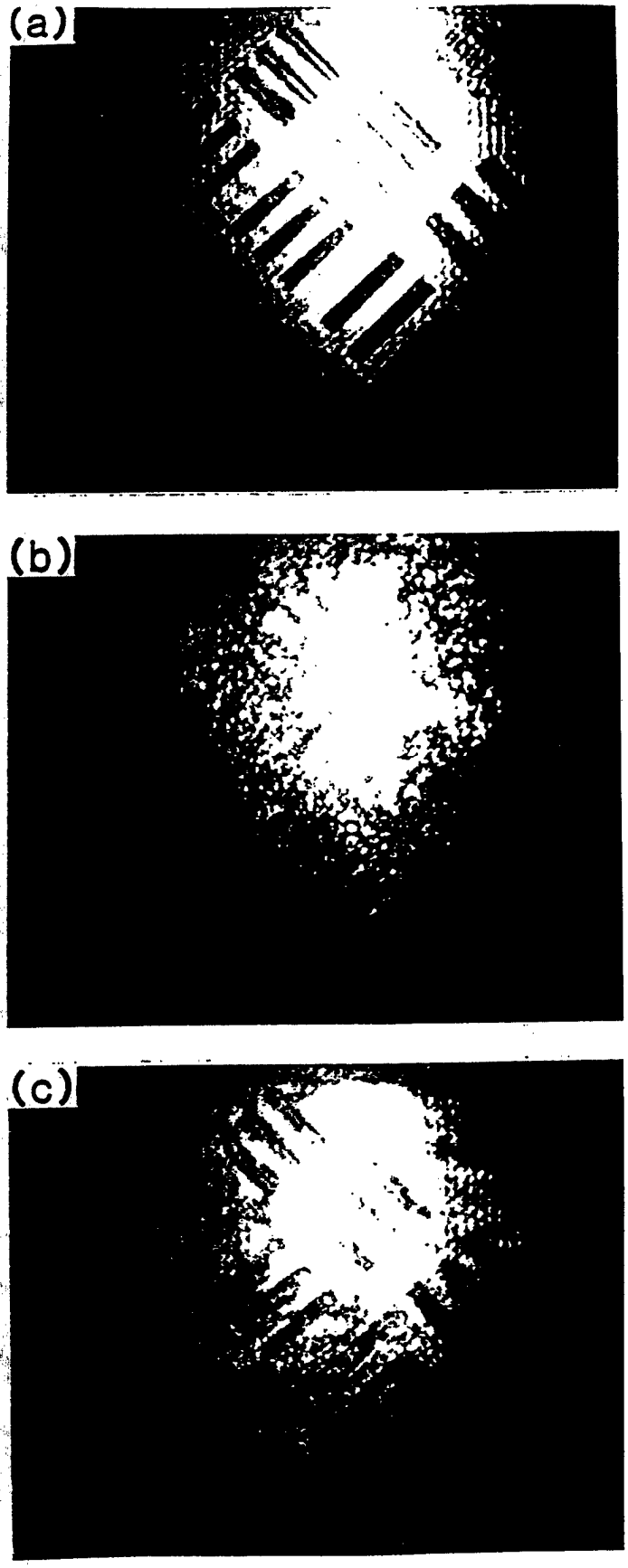
(a)
(b)
(c)

5. APPENDIX

5. PUBLICATIONS

2.4.1 (a) JOURNAL PUBLICATIONS:

(1) G. Asimellis, J. Khoury and Charles L. Woods, "Effect of saturation on the nonlinear joint incoherent erasure joint transform correlator," JOSA A: 13, (1996)

5.4.1.(b) PRESENTATIONS:

(1) J. Khoury, Jonathan S. Kane, Philip R. Hemmer and Charles L. Woods, "Homodyne detection for imaging in a scattering medium," Paper TuY3

(2) George Asimelis, J. Khoury and Charles L. Woods, "Tunable nonlinear incoherent erasure joint transform correlator," Paper Thww3. OSA meeting, Rochester NY, (1996).

(3) George Asimelis, J. Khoury and Charles L. Woods, "Performance of nonlinear joint transform correlator with noisy inputs," Paper ThWW4. OSA, Meeting Rochester, NY 1996.

(4) "Photorefractive incoherent-erasure joint transform correlator," Technical Digest "Photorefractive Fiber and Crystal Devices: Materials, Optical Properties, and Applications " SPIE, August 1996 Abstract.

5.4.2 PATENTS:

1- Homodyne and heterodyne imaging in a scattering medium

2- Imaging in a scattering medium using photon density waves.